The novel hybrid agonist HyNDA-1 targets the D3R-nAChR heteromeric complex in dopaminergic neurons

Carlo Matera,[a,#,1] Federica Bono,[b,1] Silvia Pelucchi,[c] Ginetta Collo,[b] Leonardo Bontempi,[b] Cecilia Gotti,[d] Michele Zoli,[e] Marco De Amici,[a] Cristina Missale,[b] Chiara Fiorentini,[b,2,*] Clelia Dallanoce[a,2,*]

[a]*Dipartimento di Scienze Farmaceutiche - Sezione di Chimica Farmaceutica "Pietro Pratesi", Università degli Studi di Milano, Via L. Mangiagalli 25, 20133 Milano, Italy*

[b]*Dipartimento di Medicina Molecolare e Traslazionale - Sezione di Farmacologia, Università degli Studi di Brescia, Viale Europa 11, 25123 Brescia, Italy*

[c]*Dipartimento di Scienze Farmacologiche e Biomolecolari, Università degli Studi di Milano, Via Balzaretti 9, 20133 Milano, Italy*

[d]*Istituto di Neuroscienze, CNR, Via Vanvitelli 32, 20129 Milan, Italy*

[e]*Dipartimento di Scienze Biomediche, Metaboliche e Neuroscienze, Università degli Studi di Modena e Reggio Emilia, Via G. Campi 287, 41125 Modena, Italy*

[#]*Present address: Institute for Bioengineering of Catalonia (IBEC), Barcelona Institute of Science and Technology (BIST), Carrer Baldiri Reixac 15-21, 08028 Barcelona, Spain*

[1]Contributed equally to the work.

[2]Contributed equally as senior authors.

*Corresponding authors:

E-mail address: clelia.dallanoce@unimi.it (C. Dallanoce), chiara.fiorentini@unibs.it (C. Fiorentini)

A B S T R A C T

In this paper, we designed, synthesized and tested a small set of three new derivatives potentially targeting the D3R-nAChR heteromer, a receptor complex recently identified and characterized as the molecular entity that, in dopaminergic neurons, mediates the neurotrophic effects of nicotine. By means of a partially rigidified spacer of variable length, we incorporated in the new compounds (**1a-c**) the pharmacophoric substructure of a known β2-subunit-containing nAChR agonist (A-84543) and that of the D2/D3R agonist drug ropinirole. All the compounds retained the ability to bind with high affinity both β2-subunit-containing nAChR and D3R. Compound **1a**, renamed **HyNDA-1**, which is characterized by the shortest linker moiety, was the most interesting ligand. We found, in fact, that **HyNDA-1** significantly modulated structural plasticity on both mice and human dopaminergic neurons, an effect strongly prevented by co-incubating this ligand with either nAChR or D3R antagonists. Moreover, the neurotrophic effects of **HyNDA-1** were specifically lost by disrupting the complex with specific interfering peptides. Interestingly, by using the Bioluminescence Resonance Energy Transfer 2 ($BRET^2$) assay in HEK-293 transfected cells, we also found that **HyNDA-1** has the ability to increase the affinity of interaction between nAChR and D3R. Overall, our results indicate that the neurotrophic effects of **HyNDA-1** are mediated by activation of the D3R-nAChR heteromeric complex specifically expressed on dopaminergic neurons.

Keywords:

Hybrid **N**icotinic **D**opaminergic **A**gonist (**HyNDA**)

Receptor heteromers

Rational drug design

Dopaminergic neurons

Neurotrophic effects

1. Introduction

G protein-coupled receptors (GPCRs), which represent the largest family of membrane-bound proteins involved in the intracellular translation of extracellular stimuli, were believed to exist only as functional monomeric/homomeric receptors [1]. However, in the last two decades, accumulating evidence suggests that GPCRs may form heterodimers or larger oligomeric architectures whose functional significance is still debated and often needs further investigation [2-4]. Nevertheless, this propensity of GPCRs to physically interact with other members of the same family or with functionally and structurally divergent receptors, such as ion channels, may engender unique pharmacological, signaling and trafficking properties [2-4]. Since heteromers represent specific functional units, heteromerization provides the framework to explain how signals are integrated at the plasma membrane and to develop putative lead compounds specifically targeting these receptor complexes [5,6]. In this context, the five dopamine (DA) receptors, belonging to the GPCR family and classified as D1-like (D1 and D5) and D2-like (D2, D3 and D4) receptors, were found to form a variety of heteromers [7-10], thus providing new insight into the physiological and pathophysiological processes involving DA and expanding the potential of DA transduction machinery.

Mammalian nicotinic acetylcholine receptors (nAChRs) are a large family of ligand-gated ion channels (LGICs) and are highly expressed in the central nervous system (CNS) as pentameric assemblies of various α (α1-α10) and β (β1-β4) subunits. nAChRs give rise to functional heteromeric and homomeric channels, which contribute to processes like neurotransmitter release and synaptic plasticity [11-13]. In particular, the α4β2 receptor channel is the most abundant in the CNS and is the principal functional nAChR subtype in DA neuron somatodendritic area [14]. Based on proteomic, biophysical, and functional evidence, a crosstalk of nAChRs with GPCRs and G proteins has been demonstrated in various systems [15-17]. Interestingly, the interaction between nicotinic acetylcholine and DA neurotransmitter systems has been found to be crucial for inducing long-term depression of synaptic efficacy in dorsal striatum [18]. Moreover, a functional crosstalk between β2*nAChRs and the DA D2 receptor (D2R) was observed at presynaptic terminals of the ventral striatum, where these receptors regulate DA release and are involved in the nicotine-mediated reward behavior in rodents [19]. In addition, both nAChR and the DA D3 receptor (D3R) are co-expressed in DA neurons where they synergistically act to promote DA neuron structural plasticity [20,21]. Recently, a heteromeric, constitutive complex formed by β2*nAChR and D3R has been identified in transfected cell systems and mouse DA neurons

as the molecular entity mediating the neurotrophic effects of nicotine on DA neurons [21]. Therefore, the D3R-nAChR complex may represent a molecular target for drugs acting on DA neurons to modulate their plasticity and survival in different pathological conditions [21,22]. Although the functional properties of such a receptor complex require further studies, this achievement could be a relevant step forward to clarify the molecular basis of the neurotrophic effects of nicotine. Characterization of the D3R-nAChR heteromer as a novel pharmacological target implies that negative or positive modulators could be designed to either counteract or stimulate this receptor complex. As a first step, we aimed at identifying hybrid activators, i.e. agonists able to target both interacting receptor subtypes. The study of biologically active hybrid derivatives has characterized our research efforts in the field of muscarinic acetylcholine receptors (mAChRs), since we rationally conceived bitopic molecular probes, i.e. novel ligands simultaneously targeting the orthosteric and the allosteric binding site of M2 mAChRs [23-25]. Moreover, we synthesized and tested a group of bifunctional ligands targeting both nAChR and DA receptor (DAR) subtypes, which essentially combined the pharmacological profile of their individual parent compounds [26].

The combination of complementary pharmacological actions inside new individual chemical entities follows different approaches, leading to hybrid, fused or chimeric ligands [27-30]. In this framework, bivalent ligands are those compounds incorporating two pharmacophoric moieties linked by a spacer, whose molecular skeleton is designed for simultaneous binding to both receptor proteins of a dimer. On the other hand, dual-acting ligands combine two pharmacophoric units, linked by usually shorter spacers than those associated to bivalent ligands, and are not meant for simultaneous binding to a given dimeric receptor [31,32]. In general, as much as the structure of the two parent pharmacologically active compounds is merged, producing integrated compounds, a gain in the drug-like properties of the new ligands is acquired, mainly in terms of reduction of molecular mass, lipophilicity and polar surface area, thus favoring their ability to reach the CNS [31,32].

The general criteria for choosing the parent structures to be used as pharmacophoric units of a hybrid ligand are (1) a favorable pharmacological profile (i.e., high binding affinity to and selectivity for the target individual receptors), (2) structural simplicity and synthetic accessibility, (3) a certain degree of drug-likeness, and (4) the ability to tolerate relatively bulky substituents at the site of connection to the partner unit without losing binding affinity. With these criteria in mind, we selected the nAChR and D3R agonist building blocks

after an accurate analysis of the literature. The choice of A-84543 [33] was further supported by studies demonstrating the ability of the C5 position of the pyridyl moiety of this α4β2 nAChR agonist to tolerate sterically bulky substituents without losing binding affinity or even increasing selectivity for the α4β2 subtype [34]. In particular, a set of A-84543 analogues containing hydrogen-bonding alkynyl substituents at the C5 position showed an exceptionally high selectivity for nAChRs containing β2 subunits over receptors containing β4 subunits [35] (Fig. 1). Accordingly, we used such a position and an alkynyl chain as a site for the merger with the D3R agonist moiety. For the dopaminergic molecular portion of our ligands, we considered that ropinirole (Fig. 1), despite its relatively low subtype selectivity, is a D2-like receptor agonist with a D3R-preferring profile [36], displaying a nanomolar affinity for the D3R subtype. In addition, evidence suggests its pivotal role in promoting survival and neurotrophic effects on midbrain DA neurons by regulating the release of endogenous neurotrophic factors such as GDNF and BDNF, mainly through activation of D3R [37]. Furthermore, ropinirole has already been successfully employed in the development of homo- and hetero-bivalent as well as integrated dual-acting ligands [31,38], and this suggested to which extent modifications of its molecular skeleton might affect its former pharmacological profile.

Figure 1 *about here*

Having identified our ideal candidate structures, we designed the set of three putative hybrid D3R-(β2*) nAChR agonists **1a** [from now on identified as **HyNDA** (**Hy**brid **N**icotinic **D**opaminergic **A**gonist)**-1**], **1b** and **1c** (Fig. 1), which show different degrees of molecular integration. To this end, we linked the two pharmacophores through partially rigidified spacers of different length by taking into account the results obtained by Kozikowski et al. [35], which expanded the pharmacophoric moiety of A-84543 at the C5 position of the pyridine ring, as illustrated in Fig. 1. The target compounds were thus synthesized and assessed for their binding properties at the target receptors and their functional activity in both mouse and human midbrain DA neurons.

2. Material and methods

2.1. Reagents, drugs and synthetic protocols

All chemicals were purchased from Sigma-Aldrich Srl (Milan, Italy) and were used without further purification except when mentioned specifically. [^{3}H]Epibatidine (Epi, specific activity 56-65 Ci/mmol)

[^{125}I]α-bungarotoxin (α-Bgtx, specific activity 112 Ci/mmol) and ^{3}[H]sulpiride (72.2 Ci/mmol) were purchased from Perkin-Elmer (Waltham, MA, USA). Nonradioactive α-Bgtx, epibatidine, nicotine sulfate, mecamylamine, phenylmethylsulfonyl fluoride, EDTA, EGTA, NaCl, KCl, $MgSO_4$, $CaCl_2$ and polyethylenimine were purchased from Sigma-Aldrich. Ropinirole, dihydro-β-erythroidine hydrobromide and quinpirole were purchased from Tocris. 3-(1-Methyl-2(*S*) pyrrolidinyl)methoxy)pyridine fumarate (A-84543) was prepared according to a published procedure [33]; all analytical data of the synthesized compound matched those reported in the literature.

All reactions were performed under inert atmosphere (argon or nitrogen) and glassware was oven-dried or flame-dried prior to use. The reactions were monitored by thin-layer chromatography (TLC) on commercial aluminum plates precoated with silica gel 60 (F-254, Merck). Visualization was performed with UV light at 254 nm; spots were further evidenced by spraying with a dilute alkaline potassium permanganate solution or a phosphomolybdic acid solution and, for tertiary amines, with the Dragendorff reagent. The synthesized compounds were purified on glass flash chromatography columns packed with silica gel (230-400 mesh particle size, pore size 60 Å, Merck). Melting points of solid products were measured in capillary tubes with a model B 540 Büchi apparatus and are uncorrected. Optical rotations were measured with a Jasco P-1010 Polarimeter (sodium D line, 589 nm) coupled with a Huber thermostat (20 °C). ^{1}H NMR and ^{13}C NMR spectra were recorded with a Varian Mercury 300 (^{1}H, 300.063; ^{13}C, 75.451 MHz) spectrometer at 25 °C; coupling constants (*J*) are given in Hz; chemical shifts (δ) are expressed in ppm and were calibrated for ^{1}H using TMS and for ^{13}C using residual deuterated solvent as internal standard. Abbreviations used for peak multiplicities are the following: s (singlet), bs (broad singlet), d (doublet), t (triplet), q (quartet), m (multiplet), dd (doublet of doublets), dt (doublet of triplets), td (triplet of doublets), app t (apparent triplet). ESI mass spectra were obtained on a Varian 320 LC-MS/MS instrument; data are reported as mass-to-charge ratio (m/z) of the corresponding positively charged molecular ions. Microanalyses (C, H, N) of the final compounds agreed with the theoretical value within ± 0.4%.

*2.1.1. (S)-3-Bromo-5-((1-methylpyrrolidin-2-yl)methoxy)pyridine (**2**)*

To a stirred solution of (*S*)-1-metyl-2-pyrrolidinylmethanol (3.5 g, 30 mmol) in anhydrous DMF (150 ml) was added NaH (60% in mineral oil, 1.8 g, 46 mmol) in small portions. The reaction mixture was stirred at

room temperature for 2 h, then 3,5-dibromopyridine (10.8 g, 46 mmol) was added and the color turned to orange in a few minutes. After vigorous stirring at room temperature for additional 48 h, the reaction mixture was poured into ice-water (350 ml) and extracted with CH_2Cl_2 (200 ml × 3). The combined organic layers were washed with brine, dried over anhydrous Na_2SO_4 and evaporated under reduced pressure. The residue was purified by flash chromatography with CH_2Cl_2/MeOH (95:5) to afford **2** as a brown oil (6.1 g). Yield: 74%. $[\alpha]^{20}_D$ –40 (c = 1.50, $CHCl_3$). ^{1}H NMR ($CDCl_3$) δ 8.25 (d, 1H, J = 1.7 Hz), 8.23 (d, 1H, J = 2.5 Hz), 7.36 (t, 1H, J = 2.5 Hz), 3.98 (dd, 1H, J = 9.4, 5.2 Hz), 3.90 (dd, 1H, J = 9.4, 5.2 Hz), 3.12-3.06 (m, 1H), 2.69-2.60 (m, 1H), 2.45 (s, 3H), 2.29 (td, 1H, J = 9.4, 7.4 Hz), 2.04-1.95 (m, 1H), 1.88-1.64 (m, 3H). ^{13}C NMR ($CDCl_3$) δ 155.71, 143.14, 136.69, 124.18, 120.57, 71.73, 64.22, 57.92, 41.94, 28.76, 23.31. ESI-MS calculated for $C_{11}H_{16}BrN_2O^+$ $[M+H]^+$ 271.04, found 271.0.

*2.1.2. (S)-6-(5-((1-Methylpyrrolidin-2-yl)methoxy)pyridin-3-yl)hex-5-yn-1-ol (**3a**)*

A mixture of **2** (914 mg, 3.37 mmol), 10% Pd-C (100 mg), CuI (103 mg, 0.539 mmol), K_2CO_3 (1.16 g, 8.43 mmol) and PPh_3 (97 mg, 0.371 mmol) in DME (7 ml) and H_2O (7 ml) was stirred under argon for 30 min. 5-Hexyn-1-ol (827 mg, 8.43 mmol) was then added and the reaction mixture was heated under reflux for 72 h. The cooled mixture was then filtered through a Celite pad and the filtrate was concentrated in vacuo. The residue was purified by flash chromatography with CH_2Cl_2/MeOH (9:1) to afford **3a** as a yellow oil (840 mg). Yield: 86%. $[\alpha]^{20}_D$ –38 (c = 1.50, $CHCl_3$). ^{1}H NMR ($CDCl_3$) δ 8.21 (d, 1H, J = 1.4 Hz), 8.20 (d, 1H, J = 2.7 Hz), 7.19 (dd, 1H, J = 2.7, 1.4 Hz), 3.99 (dd, 1H, J = 9.4, 5.5 Hz), 3.92 (dd, 1H, J = 9.4, 5.5 Hz), 3.70 (t, 2H, J = 6.1 Hz), 3.16-3.10 (m, 1H), 2.72-2.63 (m, 1H), 2.49 (s, 3H), 2.46 (t, 2H, J = 6.1 Hz), 2.31 (td, 1H, J = 9.4, 7.5 Hz), 2.08-1.98 (m, 1H), 1.91-1.63 (m, 7H). ^{13}C NMR ($CDCl_3$) δ 154.52, 144.54, 136.94, 123.22, 121.23, 93.51, 77.54, 71.15, 64.12, 62.02, 57.75, 41.77, 31.92, 28.55, 24.91, 23.01, 19.25. ESI-MS calculated for $C_{17}H_{25}N_2O_2^+$ $[M+H]^+$ 289.19, found 289.2.

*2.1.3. (S)-8-(5-((1-Methylpyrrolidin-2-yl)methoxy)pyridin-3-yl)oct-7-yn-1-ol (**3b**)*

Compound **3b** was prepared in a similar fashion as described for **3a**, combining **2** (907 mg, 3.34 mmol), 10% Pd-C (99 mg), CuI (102 mg, 0.535 mmol), K_2CO_3 (1.16 g, 8.36 mmol), PPh_3 (97 mg, 0.368 mmol) and 7-octyn-1-ol (1.06 g, 8.36 mmol) in DME (7 ml) and H_2O (7 ml). The crude target compound was purified by

flash chromatography with CH_2Cl_2/MeOH (95:5) to afford **3b** as a yellow oil (824 mg). Yield: 78%. $[\alpha]^{20}_D$ –41 (c = 0.90, $CHCl_3$). ^{1}H NMR ($CDCl_3$) δ 8.20 (d, 1H, *J* = 1.1 Hz), 8.19 (d, 1H, *J* = 3.0 Hz), 7.18 (dd, 1H, *J* = 3.0, 1.1 Hz), 3.99 (dd, 1H, *J* = 9.4, 5.5 Hz), 3.90 (dd, 1H, *J* = 9.4, 5.5 Hz), 3.65 (t, 2H, *J* = 6.3 Hz), 3.14-3.08 (m, 1H), 2.71-2.62 (m, 1H), 2.47 (s, 3H), 2.42 (t, 2H, *J* = 6.9 Hz), 2.31 (td, 1H, *J* = 9.4, 7.4 Hz), 2.06-1.96 (m, 1H), 1.89-1.67 (m, 3H), 1.64-1.55 (m, 4H), 1.53-1.35 (m, 4H). ^{13}C NMR ($CDCl_3$) δ 154.72, 144.85, 137.22, 123.40, 121.48, 93.95, 77.60, 71.40, 64.38, 63.01, 57.94, 41.94, 32.86, 28.90, 28.79, 28.67, 25.54, 23.25, 19.59. ESI-MS calculated for $C_{19}H_{29}N_2O_2^+$ $[M+H]^+$ 317.22, found 317.2.

*2.1.4. (S)-10-(5-((1-Methylpyrrolidin-2-yl)methoxy)pyridin-3-yl)dec-9-yn-1-ol (**3c**)*

Compound **3c** was prepared in a similar fashion as described for **3a**, combining **2** (936 mg, 3.45 mmol), 10% Pd-C (103 mg), CuI (105 mg, 0.552 mmol), K_2CO_3 (1.19 g, 8.63 mmol), PPh_3 (100 mg, 0.380 mmol) and 9-decyn-1-ol (1.33 g, 8.63 mmol) in DME (7 ml) and H_2O (7 ml). The crude target compound was purified by flash chromatography with CH_2Cl_2/MeOH (95:5) to afford **3c** as a yellow oil (881 mg). Yield: 74%. $[\alpha]^{20}_D$ –26 (c = 0.80, $CHCl_3$). ^{1}H NMR ($CDCl_3$) δ 8.12 (s, 1H), 8.10 (d, 1H, *J* = 2.5 Hz), 7.12 (s, 1H), 3.95 (dd, 1H, *J* = 9.4, 5.5 Hz), 3.85 (dd, 1H, *J* = 9.4, 5.5 Hz), 3.51 (t, 2H, *J* = 6.6 Hz), 3.09-3.03 (m, 1H), 2.69-2.61 (m, 1H), 2.41 (s, 3H), 2.32 (t, 2H, *J* = 6.9 Hz), 2.26 (td, 1H, *J* = 9.4, 7.7 Hz), 2.02-1.90 (m, 1H), 1.82-1.58 (m, 3H), 1.56-1.43 (m, 4H), 1.40-1.32 (m, 2H), 1.31-1.20 (m, 6H). ^{13}C NMR ($CDCl_3$) δ 154.59, 144.70, 137.02, 123.36, 121.58, 94.19, 77.82, 70.97, 64.47, 62.61, 57.80, 41.79, 32.97, 29.46, 29.19, 28.90, 28.64, 28.58, 25.97, 23.09, 19.55. ESI-MS calculated for $C_{21}H_{33}N_2O_2^+$ $[M+H]^+$ 345.25, found 345.2.

*2.1.5. (S)-6-(5-((1-Methylpyrrolidin-2-yl)methoxy)pyridin-3-yl)hex-5-ynal (**4a**)*

Dess-Martin periodinane (1.49 g, 3.52 mmol) was added to a stirred solution of alcohol **3a** (780 mg, 2.70 mmol) in CH_2Cl_2 (20 ml). The mixture was stirred at room temperature for 4 h and then quenched with saturated aqueous $Na_2S_2O_3$ solution (10 ml) followed by saturated aqueous $NaHCO_3$ solution (10 ml). The organic layer was separated and the aqueous layer was further extracted with CH_2Cl_2 (50 ml × 3). The organic fractions were collected, dried over anhydrous Na_2SO_4 and evaporated under reduced pressure. The residue was purified by flash chromatography with CH_2Cl_2/MeOH (85:15) to provide **4a** as a yellow oil (652 mg). Yield: 84%. $[\alpha]^{20}_D$ –39 (c = 0.60, $CHCl_3$). ^{1}H NMR ($CDCl_3$) δ 9.77 (t, 1H, *J* = 1.4 Hz), 8.15 (bs, 2H), 7.13 (dd,

1H, *J* = 2.5, 1.7 Hz), 3.92 (dd, 1H, *J* = 9.4, 5.2 Hz), 3.85 (dd, 1H, *J* = 9.1, 5.5 Hz), 3.06-3.01 (m, 1H), 2.62-2.55 (m, 1H), 2.59 (t, 2H, *J* = 7.2 Hz), 2.44 (t, 2H, *J* = 6.9 Hz), 2.40 (s, 3H), 2.24 (dd, 1H, *J* = 16.5, 9.1 Hz), 1.99-1.89 (m, 1H), 1.93-1.83 (m, 2H), 1.79-1.58 (m, 3H). ^{13}C NMR ($CDCl_3$) δ 201.83, 154.69, 144.71, 137.41, 123.29, 120.99, 92.37, 78.50, 71.33, 64.23, 57.91, 42.90, 41.91, 28.70, 23.24, 21.13, 19.01. ESI-MS calculated for $C_{17}H_{23}N_2O_2^+$ $[M+H]^+$ 287.18, found 287.4.

*2.1.6. (S)-8-(5-((1-Methylpyrrolidin-2-yl)methoxy)pyridin-3-yl)oct-7-ynal (**4b**)*

Compound **4b** was prepared in a similar fashion as described for **4a**, combining **3b** (723 mg, 2.28 mmol) and Dess-Martin periodinane (1.26 g, 2.97 mmol) in CH_2Cl_2 (20 ml). The crude target compound was purified by flash chromatography with CH_2Cl_2/MeOH (85:15) to afford **4b** as a yellow oil (644 mg). Yield: 90%. $[\alpha]^{20}_D$ –42 (c = 0.95, $CHCl_3$). ^{1}H NMR ($CDCl_3$) δ 9.74 (t, 1H, *J* = 1.6 Hz), 8.17 (bs, 2H), 7.15 (d, 1H, *J* = 1.7 Hz), 3.97 (dd, 1H, *J* = 9.4, 5.5 Hz), 3.88 (dd, 1H, *J* = 9.4, 5.5 Hz), 3.12-3.06 (m, 1H), 2.68-2.60 (m, 1H), 2.48-2.35 (m, 4H), 2.44 (s, 3H), 2.28 (dd, 1H, *J* = 16.5, 9.1 Hz), 2.05-1.92 (m, 1H), 1.86-1.69 (m, 3H), 1.67-1.53 (m, 4H), 1.51-1.38 (m, 2H). ^{13}C NMR ($CDCl_3$) δ 202.68, 154.67, 144.81, 137.25, 123.31, 121.32, 93.50, 71.21, 64.33, 57.89, 43.95, 41.88, 29.90, 28.70, 28.54, 28.42, 23.23, 21.75, 19.45. ESI-MS calculated for $C_{19}H_{27}N_2O_2^+$ $[M+H]^+$ 315.21, found 315.3.

*2.1.7. (S)-10-(5-((1-Methylpyrrolidin-2-yl)methoxy)pyridin-3-yl)dec-9-ynal (**4c**)*

Compound **4c** was prepared in a similar fashion as described for **4a**, combining **3c** (830 mg, 2.41 mmol) and Dess-Martin periodinane (1.33 g, 3.13 mmol) in CH_2Cl_2 (20 ml). The crude target compound was purified by flash chromatography with CH_2Cl_2/MeOH (85:15) to afford **4c** as a yellow oil (667 mg). Yield: 81%. $[\alpha]^{20}_D$ –32 (c = 1.15, $CHCl_3$). ^{1}H NMR ($CDCl_3$) δ 9.69 (t, 1H, *J* = 1.6 Hz), 8.14 (bs, 2H), 7.12 (d, 1H, *J* = 0.8 Hz), 3.91 (dd, 1H, *J* = 9.1, 5.5 Hz), 3.84 (dd, 1H, *J* = 9.4, 5.5 Hz), 3.06-3.00 (m, 1H), 2.63-2.54 (m, 1H), 2.43-2.29 (m, 4H), 2.40 (s, 3H), 2.23 (dd, 1H, *J* = 16.5, 9.1 Hz), 2.01-1.89 (m, 1H), 1.81-1.65 (m, 3H), 1.63-1.46 (m, 4H), 1.42-1.33 (m, 2H), 1.31-1.25 (m, 4H). ^{13}C NMR ($CDCl_3$) δ 202.90, 154.69, 144.78, 137.15, 123.27, 121.37, 93.86, 71.31, 64.25, 57.89, 44.02, 41.87, 32.72, 29.18, 29.03, 28.83, 28.71, 28.59, 23.23, 22.17, 19.56. ESI-MS calculated for $C_{21}H_{31}N_2O_2^+$ $[M+H]^+$ 343.24, found 343.4.

*2.1.8. 4-(2-Hydroxyethyl)indolin-2-one (**5**)*

Intermediate **5** was obtained following a five-step synthetic procedure that we previously described [39], starting from commercially available 2-(2-methyl-3-nitrophenyl)acetic acid. Mp: 146-148 °C (white powder, crystallized from CH_3CN). ^{1}H NMR (CD_3OD) δ 7.13 (app t, 1H, J = 7.7 Hz), 6.86 (d, 1H, J = 7.7 Hz), 6.72 (d, 1H, J = 7.7 Hz), 3.76 (t, 2H, J = 6.6 Hz), 3.48 (s, 2H), 2.76 (t, 2H, J = 6.6 Hz). ^{13}C NMR (CD_3OD) δ 178.72, 143.14, 135.64, 127.81, 125.10, 122.85, 107.65, 61.84, 36.17, 34.95. ESI-MS calculated for $C_{10}H_{12}NO_2^+$ $[M+H]^+$ 178.09, found 178.0.

*2.1.9. 2-(2-Oxoindolin-4-yl)ethyl 4-methylbenzenesulfonate (**6**)*

To a cooled (0 °C) suspension of 4-(2-hydroxyethyl)indolin-2-one **5** (1.03 g, 5.81 mmol) and pyridine (1.38 g, 17.44 mmol) in CH_2Cl_2 (10 ml), a solution of *p*-toluenesulfonyl chloride (2.22 g, 11.63 mmol) in CH_2Cl_2 (20 ml) was added dropwise over 20 min. The reaction mixture was stirred at room temperature for 4 h and then quenched with saturated aqueous $NaHCO_3$ solution (30 ml). The organic layer was separated and the aqueous layer was further extracted with CH_2Cl_2 (100 ml × 3). The combined organic fractions were washed with brine, dried over anhydrous Na_2SO_4 and evaporated under reduced pressure. The residue was purified by flash chromatography with cyclohexane/ethyl acetate (3:7) to afford **6** as a greenish yellow solid (1.46 g). Yield: 76%. Mp: 125-127 C. ^{1}H NMR ($CDCl_3$) δ 9.36 (s, 1H); 7.62 (d, 2H, J = 8.0 Hz), 7.25 (d, 2H, J = 8.0 Hz), 7.11 (app t, 1H, J = 7.8 Hz), 6.78 (d, 1H, J = 7.4 Hz), 6.75 (d, 1H, J = 7.4 Hz), 4.22 (t, 2H, J = 6.6 Hz), 3.31 (s, 2H), 2.87 (t, 2H, J = 6.6 Hz), 2.41 (s, 3H). ^{13}C NMR ($CDCl_3$) δ 177.96, 145.16, 142.97; 132.97, 132.81, 130.06, 128.56, 127.93, 124.77, 123.11, 108.84, 69.60, 35.22, 32.82, 21.83. ESI-MS calculated for $C_{17}H_{18}NO_4S^+$ $[M+H]^+$ 332.10, found 332.0.

*2.1.10. 4-(2-(Propylamino)ethyl)indolin-2-one (**7**)*

A solution of 2-(2-oxoindolin-4-yl)ethyl 4-methylbenzenesulfonate **6** (1.20 g, 3.62 mmol) and *n*-propylamine (2.14 g, 36.21 mmol) was refluxed in a sealed tube for 1 h. The reaction mixture was then evaporated to remove excess propylamine and partitioned between CH_2Cl_2 (30 ml) and 1 M HCl solution (30 ml). The aqueous phase was basified with $NaHCO_3$ (pH≈8) and washed with CH_2Cl_2 (20 ml), then further basified with K_2CO_3 (pH≈10) and extracted with CH_2Cl_2 (30 ml × 3) to afford the title compound **7** as a yellow

oil (610 mg). Yield: 77%. ^{1}H NMR ($CDCl_3$) δ 9.31 (bs, 1H), 7.13 (app t, 1H, J = 7.7 Hz), 6.84 (d, 1H, J = 7.7 Hz), 6.72 (d, 1H, J = 7.7 Hz), 3.46 (s, 2H), 2.87 (t, 2H, J = 6.9 Hz), 2.74 (t, 2H, J = 6.9 Hz), 2.59 (t, 2H, J = 7.2 Hz), 1.53-1.44 (m, 2H), 0.89 (t, 3H, J = 7.4 Hz). ^{13}C NMR ($CDCl_3$) δ 178.27, 143.09, 136.61, 128.31, 124.49, 122.76, 108.05, 51.98, 49.69, 35.48, 33.82, 23.34, 12.02. ESI-MS calculated for $C_{13}H_{19}N_2O^+$ $[M+H]^+$ 219.15, found 219.1.

*2.1.11. (S)-4-(2-((6-(5-((1-Methylpyrrolidin-2-yl)methoxy)pyridin-3-yl)hex-5-yn-1-yl)(propyl) amino)ethyl)indolin-2-one (**HyNDA-1**)*

A solution of (*S*)-6-(5-((1-methylpyrrolidin-2-yl)methoxy)pyridin-3-yl)hex-5-ynal **4a** (341 mg, 1.19 mmol) and 4-(2-(propylamino)ethyl)indolin-2-one **7** (200 mg, 0.92 mmol) in MeOH (10 ml) was stirred at room temperature for 10 min. $NaBH_3CN$ (86 mg, 1.37 mmol) was then added and stirring was continued for 1 h. The reaction mixture was quenched with a saturated aqueous $NaHCO_3$ solution (20 ml) and extracted with CH_2Cl_2 (20 ml × 3). The organic fractions were collected, dried over anhydrous Na_2SO_4 and evaporated under reduced pressure. The residue was purified by flash chromatography with CH_2Cl_2/MeOH (4:1) to afford **1a (HyNDA-1)** as a pale yellow oil (368 mg). Yield: 82%. $[\alpha]^{20}_D$ –24 (c = 0.55, $CHCl_3$). ^{1}H NMR ($CDCl_3$) δ 9.35 (bs, 1H), 8.17 (bs, 1H), 8.16 (d, 1H, J = 1.4 Hz), 7.16-7.14 (m, 1H), 7.08 (app t, 1H, J = 7.7 Hz), 6.80 (d, 1H, J = 7.7 Hz), 6.68 (d, 1H, J = 7.7 Hz), 4.01 (dd, 1H, J = 9.4, 5.2 Hz), 3.92 (dd, 1H, J = 9.4, 5.2 Hz), 3.44 (s, 2H), 3.17-3.11 (m, 1H), 2.75-2.65 (m, 5H), 2.57-2.53 (m, 2H), 2.51-2.46 (m, 2H), 2.49 (s, 3H), 2.43-2.39 (m, 2H), 2.33 (dd, 1H, J = 16.8, 9.4 Hz), 2.07-1.93 (m, 1H), 1.92-1.67 (m, 4H), 1.65-1.55 (m, 3H), 1.53-1.45 (m, 2H), 0.88 (t, 3H, J = 7.4 Hz). ^{13}C NMR ($CDCl_3$) δ 177.66, 154.64, 144.82, 142.95, 137.15, 137.01, 128.25, 124.29, 123.36, 122.86, 121.37, 107.80, 93.67, 77.80, 70.95, 64.53, 57.88, 56.22, 54.21, 53.53, 41.89, 35.37, 30.70, 28.62, 26.50, 26.34, 23.24, 20.33, 19.54, 12.17. ESI-MS calculated for $C_{30}H_{41}N_4O_2^+$ $[M+H]^+$ 489.32, found 489.3, and for $C_{30}H_{42}N_4O_2^{2+}$ $[M+2H]^{2+}$ 490.33, found 245.3. Anal. Calcd for $C_{30}H_{40}N_4O_2$ (488.66): C, 73.74; H, 8.25; N, 11.47. Found: C, 73.49; H, 8.02; N, 11.16.

*2.1.12. (S)-4-(2-((8-(5-((1-Methylpyrrolidin-2-yl)methoxy)pyridin-3-yl)oct-7-yn-1-yl)(propyl) amino)ethyl)indolin-2-one (**1b**)*

Compound **1b** was prepared in a similar fashion as described for **1a**, combining **4b** (350 mg, 1.11 mmol), 4-(2-(propylamino)ethyl)indolin-2-one **7** (187 mg, 0.86 mmol) and $NaBH_3CN$ (81 mg, 1.28 mmol) in MeOH (10 ml). The crude target compound was purified by flash chromatography with CH_2Cl_2/MeOH (85:15) to afford **1b** as a pale yellow oil (352 mg). Yield: 80%. $[\alpha]^{20}_D$ –23 (c = 0.45, $CHCl_3$). ^{1}H NMR ($CDCl_3$) δ 8.71 (bs, 1H), 8.20 (bs, 1H), 8.18 (d, 1H, *J* = 2.8 Hz), 7.19-7.17 (m, 1H), 7.13 (app t, 1H, *J* = 7.7 Hz), 6.83 (d, 1H, *J* = 7.7 Hz), 6.70 (d, 1H, *J* = 7.7 Hz), 4.02 (dd, 1H, *J* = 9.1, 5.5 Hz), 3.93 (dd, 1H, *J* = 9.1, 5.5 Hz), 3.47 (s, 2H), 3.17-3.12 (m, 1H), 2.75-2.65 (m, 4H), 2.60-2.42 (m, 4H), 2.50 (s, 3H), 2.41 (t, 2H, *J* = 6.9 Hz), 2.34 (dd, 1H, *J* = 16.8, 9.4 Hz), 2.10-1.95 (m, 1H), 1.92-1.67 (m, 3H), 1.65-1.56 (m, 2H), 1.55-1.38 (m, 5H), 1.37-1.28 (m, 2H), 1.27-1.20 (m, 2H), 0.88 (t, 3H, *J* = 7.4 Hz). ^{13}C NMR ($CDCl_3$) δ 177.45, 154.66, 144.85, 142.82, 137.21, 137.07, 128.30, 124.28, 123.32, 122.94, 121.47, 107.78, 93.96, 77.70, 71.13, 64.48, 57.89, 56.15, 54.23, 54.07, 41.91, 35.32, 30.65, 29.01, 28.73, 28.69, 27.20, 26.86, 23.27, 20.18, 19.62, 12.14. ESI-MS calculated for $C_{32}H_{45}N_4O_2^+$ $[M+H]^+$ 517.35, found 517.4, and for $C_{32}H_{46}N_4O_2^{2+}$ $[M+2H]^{2+}$ 518.36, found 259.5. Anal. Calcd for $C_{32}H_{44}N_4O_2$ (516.72): C, 74.38; H, 8.58; N, 10.84. Found: 74.59; H, 8.79; N, 11.12.

*2.1.13. (S)-4-(2-((10-(5-((1-Methylpyrrolidin-2-yl)methoxy)pyridin-3-yl)dec-9-yn-1-yl)(propyl) amino)ethyl)indolin-2-one (**1c**)*

Compound **1c** was prepared in a similar fashion as described for **1a**, combining **4c** (392 mg, 1.14 mmol), 4-(2-(propylamino)ethyl)indolin-2-one **7** (192 mg, 0.88 mmol) and $NaBH_3CN$ (83 mg, 1.32 mmol) in MeOH (10 ml). The crude target compound was purified by flash chromatography with CH_2Cl_2/MeOH (9:1) to afford **1c** as a pale yellow oil (371 mg). Yield: 77%. $[\alpha]^{20}_D$ –23 (c = 0.55, $CHCl_3$). ^{1}H NMR ($CDCl_3$) δ 9.27 (bs, 1H), 8.19 (d, 1H, *J* = 1.4 Hz), 8.17 (d, 1H, *J* = 2.8 Hz), 7.18-7.16 (m, 1H), 7.14 (app t, 1H, *J* = 7.7 Hz), 6.82 (d, 1H, *J* = 7.7 Hz), 6.69 (d, 1H, *J* = 7.7 Hz), 3.98 (dd, 1H, *J* = 9.1, 5.5 Hz), 3.90 (dd, 1H, *J* = 9.4, 5.5 Hz), 3.45 (s, 2H), 3.13-3.07 (m, 1H), 2.71-2.61 (m, 4H), 2.51-2.42 (m, 4H), 2.46 (s, 3H), 2.39 (t, 2H, *J* = 6.9 Hz), 2.30 (dd, 1H, *J* = 16.8, 9.4 Hz), 2.07-1.95 (m, 1H), 1.91-1.66 (m, 3H), 1.64-1.52 (m, 2H), 1.51-1.36 (m, 5H), 1.36-1.19 (m, 8H), 0.87 (t, 3H, *J* = 7.4 Hz). ^{13}C NMR ($CDCl_3$) δ 177.76, 154.71, 144.81, 142.90, 137.26, 137.14, 128.23, 124.29, 123.36, 122.94, 121.52, 107.72, 94.11, 77.73, 71.31, 64.39, 57.90, 56.30, 54.38, 54.27, 41.91, 35.38, 30.91, 29.66, 29.34, 29.08, 28.78, 28.74, 27.72, 27.20, 23.27, 20.43, 19.65, 12.18. ESI-MS calculated for

$C_{34}H_{49}N_4O_2^+$ $[M+H]^+$ 545.39, found 545.4. Anal. Calcd for $C_{34}H_{48}N_4O_2$ (544.77): C, 74.96; H, 8.88; N, 10.28. Found: C, 74.75; H, 8.72; N, 10.22.

2.2. Receptor binding assays

2.2.1. Binding to nicotinic receptor subtypes

The affinity (K_i) of the synthetized compounds for the α4β2 and α7 nAChRs was assessed in vitro using [^{3}H]epibatidine-labelled rat cerebral cortex membranes and [^{125}I]α-bungarotoxin-labelled rat hippocampus membranes, respectively. Frozen cortex and hippocampus specimens were taken from adult male Sprague-Dawley rats (275-300 g), obtained from Charles River Laboratories (Calco, Italy). All of the animal experiments were performed in accordance with the Directive 2010/63/EU. Native nAChRs and heterologously expressed human α3β4 nAChRs were prepared as previously described [26]. Nonspecific [^{125}I]α-bungarotoxin binding was determined in parallel by means of incubation in the presence of 1 μM unlabelled α-bungarotoxin, whereas non-specific [^{3}H]epibatidine binding was determined by incubation with 10 nM epibatidine. The inhibition of [^{3}H]epibatidine and [^{125}I]α-bungarotoxin binding was measured by incubating the samples with increasing concentrations of each compound for five minutes followed by overnight incubation at 4 °C, with [^{3}H]epibatidine 0.1 nM (for the α4β2 subtype) or 0.25 nM (for the α3β4 subtype), or at room temperature with [^{125}I]α-bungarotoxin 1 nM in the case of the α7 subtype. After incubation, the membrane-bound α4β2, α3β4 or α7 nAChR subtypes were washed five times with ice-cold phosphate-buffered saline (PBS) (Sigma-Aldrich). [^{3}H]Epibatidine binding was determined by means of liquid scintillation counting in a β counter, and [^{125}I]α-bungarotoxin binding by means of direct counting in a γ counter.

2.2.2. Cell cultures, transfection and radioligand binding assays to D3R

Human embryonic kidney 293T (HEK-293) cells were cultured in Dulbecco's modified Eagle's medium (DMEM) containing 10% fetal bovine serum, 2 mM glutamine, 0.1 mM nonessential amino acids, 1 mM sodium pyruvate, 100 U/ml penicillin, and 100 μg/ml streptomycin (all reagents were from Euroclone, Milan, Italy) at 37 °C in an atmosphere of 5% CO_2. HEK-293 cells were transiently transfected with the human D3R-pCMV5 vector (provided by Marc Caron, Duke University, Durham, NC), using the Effectene Transfection

Reagent (Qiagen, Milan, Italy). HEK293 cells expressing D3R were homogenized with an Ultra Turrex homogenizer in 5 mM Tris-HCl containing 2 mM EDTA and a mixture of protease inhibitors, pH 7.8; the homogenate was then centrifuged at 100 × *g* for 10 min followed by the supernatant centrifugation, twice at 30,000 × *g* for 20 min at 4 °C. The resulting pellet was resuspended in 50 mM Tris-HCl containing 5 mM EDTA, 1.5 mM $CaCl_2$, 5 mM $MgCl_2$, 5 mM KCl, and 120 mM NaCl, pH 7.4, and used for radioligand binding assay. Aliquots of membrane suspension (50 µg of protein/sample) were incubated at 37 °C for 30 min with a saturating concentration (2 nM) of [^{3}H]raclopride and increasing concentrations of **HyNDA-1**, **1b** and **1c** (1 nM - 100 µM). The reactions were stopped by rapid filtration under reduced pressure through Whatman GF/C filters (Whatman, Clifton, NJ). Data were analyzed using the computer-fitting program Prism (GraphPAD Software for Science).

2.3. Animals and primary cultures of midbrain neurons

CD1 mice, obtained from Charles River Laboratory (Calco, Italy), were bred and housed in the animal-house facility of the University of Brescia with water and food ad libitum and a 12 h light-dark cycle. Animal use was in accordance with the Directive 2010/63/EU. All procedures were conformed to the National Research Guide for the Care and Use of Laboratory Animals and were approved by the Animal Research Ethical Committee of the University of Brescia. Primary cultures of midbrain neurons, typically containing 5-10% of midbrain DA (mDA) neurons, were prepared as previously described [21]. Briefly, the ventral mesencephalon was dissected from E12.5 mouse embryos, mechanically dissociated at room temperature, and suspended in Neurobasal medium (Gibco, Invitrogen, Carlsbad, CA, USA) containing 2 mM glutamine and B27 supplement (Gibco, Invitrogen). Cells were seeded on poly-D-lysine/laminin-coated coverslips and cultured at 37 °C in a humidified atmosphere of 5% CO_2 and 95% air. Half of the medium was changed every two days until treatment. Pharmacological treatments were performed after 7 days from seeding.

2.4. Human induced pluripotent stem cells (hiPSC)-derived neuronal cultures preparation

Human induced pluripotent stem cells (hiPSC) were developed from fibroblast of healthy donor and characterized as previously described [40]. Informed consent was obtained from a healthy donor prior to cell donation. The local ethics committee (CEIOC - Fatebenefratelli Hospital “San Giovanni di Dio” - Brescia,

Italy, 44/2001 and 39/2005), previously approved the consent form. A modified version of the dual-SMAD inhibition protocol was used to obtain midbrain neuronal cultures, as previously described [40]. hiPSC-derived neuronal cultures, containing ~40% of mDA neurons expressing the tyrosine hydroxylase (TH) enzyme, used as a marker of DA neurons, have been obtained following 50 days of culture.

2.5. Generation of interfering TAT-peptides

D3R-nAChR heteromer cell-permeable interfering peptides have been previously obtained and characterized and described [21]. Briefly, a 11 amino acid sequence of human immunodeficiency virus TAT transporter was linked to either the 215-225 arginine-rich region of D3R (TAT-D3R; NH_2 -YGRKKRRQRRRLKQRRRKRIL-COOH) or the 439-449 aspartate-rich region of β2 nAChR subunit (TAT-β2; NH_2-YGRKKRRQRRRHMRSEDDDQSVS-COOH) (GenScript, Piscataway, USA). Cell-permeable peptides with scrambled sequences (TAT-D3R-Sc; NH_2-YGRKKRRQRRRIRKLRLRQRK-COOH; TAT-β2-Sc; NH_2-YGRKKRRQRRRQMVDSDRHSSDE-COOH) were used as negative controls.

2.6. Treatments

For morphological analysis, primary cultures of mouse midbrain neurons were treated with nicotine (10 μM), A-84543 and ropinirole (both at 10 μM, 72 h) and with **HyNDA-1**, **1b** and **1c** at 1 μM for 72 h. In another set of experiments, midbrain neurons were incubated with different concentration of **HyNDA-1** (0.1, 0.5, 1.0 and 5.0 μM) for 72 h. In addition, neurons were incubated with **HyNDA-1** at 1.0 μM for 12, 24 and 72 h. In parallel experiments, mouse midbrain neurons were incubated for 72 h with **HyNDA-1** (1 μM) in the absence or in the presence of the D2R/D3R antagonist sulpiride (10 μM), the nonselective nAChR antagonist mecamylamine (50 μM) or the selective b2* nAChR antagonist dihydro-β-erythroidine (10 μM), added 30 min prior to **HyNDA-1** stimulation. Moreover hiPSC-derived cultures (50 days of differentiation) were incubated for 72 h with **HyNDA-1** (1 μM) in the absence or in the presence of the D2R/D3R antagonist sulpiride (10 μM), or the nonselective nAChR antagonist mecamylamine (50 μM), added 30 min prior to **HyNDA-1** stimulation. Then, mouse and human cultures were incubated with **HyNDA-1** (1 μM, 72 h) in the presence or absence of TAT-D3R and TAT-β2 peptides (both at 1 μM) and their corresponding scramble TAT-D3R Sc

and TAT-β2 Sc peptides (both at 1 μM), used as controls. Morphological analysis was conducted by immunocytochemistry (ICC) as described below.

2.7. Immunocytochemistry and computer-assisted morphology

Midbrain neurons and hiPSC-derived neuronal cultures were fixed in methanol for 10 min at 4 °C, blocked in PBS containing 0.1% Triton x-100 (Sigma-Aldrich) and 5% bovine serum albumin (BSA, Sigma-Aldrich) and incubated overnight at 4 °C with anti-TH antibody (1:500) to detect mDA neurons. Neurons were next incubated with a biotinylated anti-rabbit antibody (1:700; 30 min at room temperature) followed by a final incubation with avidin-biotin horseradish peroxidase complex. Peroxidase staining was obtained by adding 1% 3,3'-diaminobenzidine and 0.01% H_2O_2 (Sigma-Aldrich) in PBS. Digital images were acquired with an Olympus IX51 microscope connected to an Olympus digital camera. Morphometric measurements were performed by a blinded examiner on digitalized images using Image-Pro Plus software (Media Cybernetics, Bethesda, MD). The morphologic indicators of structural plasticity were: 1) maximal dendrite length, defined as the distance from the soma to the tip of the longest dendrite for each neuron; 2) primary dendrites numbers, defined as those directly stemming from the soma; 3) soma area, assessed by measuring the surface (μm^2) included by the external perimeter drawn on the cell membrane of neurons identified by TH staining. Two coverslips per treatment were examined to obtain measurements from at least 50 TH-positive mDA neurons.

2.8. Bioluminescence Resonance Energy Transfer 2 ($BRET^2$) assay

Saturation BRET assay was carried out in HEK-293 cells transfected with increasing amount of D3R-GFP construct (0.2-1.8 μg) and fixed amount of beta2-Rluc construct (0.1 μg), as previously described [21]. Twenty-four hours after transfection, cells were harvested, centrifuged, and suspended in PBS, containing 1 mg/ml D-Glucose. Cells (~45,000/well) were disseminated in a 96-well microplate (White Optiplate; Perkin Elmer) and preincubated for 5 min with **HyNDA-1** (1 μM). Deep-BlueC coelenterazine (Società Italiana Chimici, Rome) was added at the final concentration of 5 μM, and cells were analyzed for $BRET^2$ assay as previously described [21]. The BRET ratio was calculated as follow: [(emission at 515 nm)/(emission at 395 nm)] × Cf, where Cf corresponds to (emission at 515 nm)/(emission at 395 nm) for the receptor-Rluc expressed alone. $BRET^2$ saturation curves were plotted with GraphPad Prism4 (GraphPad Software, San Diego, CA),

using a linear regression curve assuming one-site binding. $BRET_{50}$ values, corresponding to the $BRET^2$ ratio at which $BRET^2$ value is 50% of the maximal level, were compared by Extra sum-of-square *F* test.

2.9. Statistical analysis

For binding experiments, the calculated binding parameters were obtained by simultaneously fitting the results of three independent experiments for each compound. The K_i values of all the tested compounds were also determined by means of the LIGAND program [41], using the data obtained from three independent saturation and competition binding experiments and compared by means of the *F* test. For morphological analyses, values are expressed as mean ± standard error of the mean (S.E.M.) if not stated otherwise. Significant differences from control conditions were determined using analysis of variance (ANOVA) followed by Bonferroni's test for multiple comparisons provided by GraphPad prism version 4.00 for Windows (GraphPad Software, San Diego, CA, USA). Correlations were assessed by calculating the correlation coefficient between two variables using the same statistical package.

3. Results

3.1. Chemistry

For the preparation of the designed ligands **1a-c** (Fig. 1), we applied a common synthetic approach varying solely the length of the alkynyl arm connecting the nicotinic portion to the dopaminergic moiety. The C5 substituted analogues of A-84543 (**3a-c**) were synthesized similarly to previously reported procedures [35]. The common nicotinic (*S*)-3-bromo-5-((1-methylpyrrolidin-2-yl)methoxy)pyridine scaffold **2** was prepared in good yield (74%) by reacting commercially available (*S*)-(1-methylpyrrolidin-2-yl)methanol and 3,5-dibromopyridine. Derivatives **3a-c** were then obtained in good yields (74-86%) by coupling **2** with the selected alkynyl spacers via a palladium-catalyzed Sonogashira reaction. To connect the nicotinic portion to the ropinirole-like fragment, we converted the terminal hydroxyl groups into the corresponding aldehydes, which afforded compounds **4a-c** in high yields (81-90%) via Dess-Martin oxidation (Fig. 2). Intermediate **5** was prepared in five steps (59% overall yield) starting from commercially available 2-(2-methyl-3-nitrophenyl)acetic acid, as previously reported by us [39]. The primary hydroxyl group in **5** was then replaced with *n*-propylamine via tosylation (compound **6**, 76% yield) to afford the ropinirole fragment **7** (77% yield)

(Fig. 2). The latter was reacted with aldehydes **4a-c** in classical reductive amination conditions, which afforded the desired target ligands **1a** (**HyNDA-1**), **1b** and **1c** (77-82% yield, Fig. 2), respectively.

Figure 2 *about here*

3.2. Binding assays

3.2.1. Binding affinities to α4β2, α3β4 and α7 nAChR subtypes

Compounds **HyNDA-1**, **1b** and **1c** and their corresponding nicotinic fragment A-84543 were assayed for binding affinity at native rat α4β2* (*indicates that the composition of the receptor is not fully established and other subunits may be present) and α7 subtypes, and to the heterologously expressed α3β4 human subtype (Table 1). As controls in each experiment, we determined the affinity of (*S*)-(-)-nicotine for the α4β2, α3β4 and α7 subtypes (K_i values equal to 2.1, 150, and 350 nM, respectively) and that of cold α-bungarotoxin (K_i = 2.5 nM) for the α7 subtype. As shown in Table 1, the affinities of **HyNDA-1**, **1b** and **1c** for the α4β2 subtype (K_i values equal to 4.50, 1.22 and1.72 nM, respectively) were all found to be comparable to that of the reference compound A-84543 *(*K_i = 1.20 nM). On the other hand, **HyNDA-1** showed higher affinity at the α3β4 subtype *(*K_i = 134 nM) than A-84543 *(*K_i = 1,900 nM) though increasing the length of the spacer significantly reduced the affinity at the α3β4 subtype (K_i values of **1b** and **1c** equal to 681 and 1,100 nM, respectively). Conversely, introduction of the spacer led to a strong reduction of the affinity of the three hybrid derivatives at the α7 subtype (K_i values of **HyNDA-1**, **1b** and **1c** equal to 11.6, 26.8 and 4.3 μM, respectively) as compared to the parent ligand A-84543 *(*K_i = 58 nM).

Table 1 *about here*

3.2.2. Binding affinities to D3R

The binding affinity of **HyNDA-1**, **1b** and **1c** for D3R was measured in HEK-293 cells transiently expressing the D3R (HEK-D3R cells). In competition experiments, membranes from HEK-D3R cells were incubated with increasing concentrations of the compounds, each tested in triplicate, with [^{3}H]raclopride as the radioligand. The competition curves derived from three separate experiments were analyzed by using the computer-fitting program Prism (GraphPad Software for Science) to obtain the K_i values (Table 1). Compounds **HyNDA-1**, **1b** and **1c** exhibited affinity for the D3R in the nanomolar range, being their K_i values

equal to 3.8, 18 and 2.6 nM, respectively. These affinities were in the same range as that of raclopride for the D3R subtype (K_i = 4.79 ± 0.85 nM) [42].

3.3. Functional assays

*3.3.1. Effects of **HyNDA-1**, **1b** and **1c** on structural plasticity in mouse mDA neurons*

As previously reported, nicotine stimulation of nAChRs expressed on DA neurons elicits neurotrophic effects [43,20]; these morphological changes have been related to the activation of the heteromeric D3R-nAChR complex [21]. The ability of hybrid compounds to exert morphological changes was investigated using primary cultures of mouse midbrain neurons, containing 5-10% of DA neurons that endogenously express D3R-nAChR heteromers [21]. In a set of preliminary experiments, midbrain neurons were incubated with **HyNDA-1**, **1b** and **1c** (1 μM, 72 h) and analyzed for morphological changes. Treatment with nicotine (10 μM, 72 h) or the individual ligands A-84543 and ropinirole (both at 10 μM, 72 h) was also performed. mDA neurons were identified by TH staining. The average maximal length of the primary dendrite, the number of dendrites and the soma area were used as indicators of structural plasticity [21].

As shown in Fig. 3, **HyNDA-1** as well as nicotine, A-84543 and ropinirole significantly increased the maximal length of the primary dendrite (Fig. 3B), the dendrite number (Fig. 3C) and the soma area (Fig. 3D) of TH-positive DA neurons, compared to untreated cells. By contrast, a broad cell toxicity was observed after **1b** and **1c** treatment (data not shown); similar results were obtained by treating neurons with lower concentrations of both compounds (0.1-0.5 μM) (data not shown). Therefore, in the subsequent experiments we used **HyNDA-1**, the only derivative in the set of the novel hybrids preserving the morphological properties of the parent ligands.

***Figure 3** about here*

*3.3.2. Dose- and time-response curves of **HyNDA-1** in mDA neurons*

The effects of **HyNDA-1** on neuronal remodeling were further investigated by incubating mouse neurons with increasing concentrations of this compound (0.1-5.0 μM) for 72 h (Fig. 4) and analyzing TH-positive neurons for morphological changes. Neurons have been also treated with nicotine (10 μM; 72 h), as control. An increase in the maximal length of the primary dendrite (Fig. 4A) and dendrite number (Fig. 4B) was

observed starting from 0.5 μM and reached the statistical significance at 1 μM. The effect of **HyNDA-1** on soma area was statistically significant starting from 0.5 μM, reaching a peak at 1 μM (Fig. 4C). However, treating neurons with **HyNDA-1** at 5 μM for 72 h resulted in cell toxicity (data not shown). Neurons were also incubated with **HyNDA-1** at 1 μM for 12, 24 and 72 h. The dendrite number was analyzed as an index of **HyNDA-1**-induced structural plasticity. A significant difference from untreated neurons was observed starting from 24 h of incubation and further increased in the following 72 h (Fig. 4D). Thus, the subsequent analyses were performed with **HyNDA-1** at 1 μM for 72 h.

Figure 4 *about here*

*3.3.3. The D3R-nAChR heteromer mediates **HyNDA-1**-induced structural plasticity in mDA neurons*

The individual role of both D3R and nAChR in **HyNDA-1**-induced neurotrophic effects was investigated by incubating mouse neurons with **HyNDA-1** (1 μM, 72 h) in the absence or presence of the D2R/D3R antagonist sulpiride (10 μM), the nonselective nAChR antagonist mecamylamine (50 μM) or the selective β2* nAChR antagonist dihydro-β-erythroidine (10 μM) [21]. Antagonists were added 30 min before **HyNDA-1** stimulation and neurons were analyzed for structural plasticity. As shown in Fig. 5 (A-D), the morphological effects of **HyNDA-1** on dendritic arborization and soma size of TH-positive neurons were prevented by D2R/D3R and nAChR antagonists; by contrast, sulpiride, mecamylamine and dihydro-β-erythroidine, when administered alone, did not produce any effect on the studied DA neuron morphological parameters. Therefore, while **HyNDA-1** may bind both D3R and β2*-subunit-containing nAChR thus activating the heteromer, blocking one or the other binding site of the complex compromises the ligand ability to induce morphological changes.

Figure 5 *about here*

The relevance of the D3R interaction with nAChR in mediating **HyNDA-1** remodeling effects was further investigated by taking advantage of two different interfering TAT-peptides, TAT-D3R and TAT-β2, previously characterized for their ability to disrupt D3R-nAChR interaction in different experimental conditions [21]. We have shown that both TAT-D3R (1 μM) and TAT-β2 (1 μM) peptides, but not their scrambled counterparts (TAT-D3R Sc and TAT-β2 Sc), abolished the neurotrophic effects of nicotine on mDA

neurons, providing a strong indication that the D3R-nAChR heteromer is the unit that specifically mediates the structural plasticity induced by nicotine [21]. On this basis, mouse midbrain cultures were treated for 72 h with **HyNDA-1** (1 μM) in the presence or the absence of either TAT-D3R or TAT-β2 or TAT-D3R Sc/TAT-β2 Sc peptides (1 μM). As reported in Fig. 6, in TH-positive mDA neurons, both TAT-D3R and TAT-β2 peptides, but not their scrambled counterparts, significantly abolished the morphological changes induced by **HyNDA-1** on dendrite length (Fig. 6B), dendrite number (Fig. 6C) and soma size (Fig. 6D). Hence, in mDA neurons, the remodeling properties shown by **HyNDA-1** are due to its targeting of both D3 and nACh receptors only when the two subtypes are assembled into the heteromeric complex.

Figure 6 *about here*

*3.3.4. Effects of **HyNDA-1** on structural plasticity of human mDA neurons*

We developed and characterized hiPSCs derived from healthy dermal fibroblasts and we differentiated these cells into mDA neurons [40]. By using this translational model, we reported that nicotine exerts morphological effects also in human mDA neurons, an effect abolished by the D2R/D3R antagonist sulpiride, which suggested the existence of a functional crosstalk between nAChR and D3R [40]. On this line, the morphological properties of **HyNDA-1** and the relevance of the D3R-nAChR complex in mediating these effects were investigated in human mDA neurons. The latter were incubated with **HyNDA-1** (1 μM, 72 h) and TH-positive neurons were analyzed for morphological remodeling. As shown in Fig. 7, **HyNDA-1** induced a significant increase of the maximal length of primary dendrite (Fig. 7B), number of dendrites (Fig. 7C) and soma area (Fig. 7D) as compared to untreated cells. Human neuronal cultures were also treated with **HyNDA-1** for 72 h in the absence or presence of sulpiride (10 μM) or mecamylamine (50 μM), both added 30 min prior to **HyNDA-1** stimulation, and mDA neurons were analyzed for structural plasticity. The results showed that blockade of either D2R/D3R or nAChR impaired the morphological effects of **HyNDA-1** (Fig. 7, A-D). Human neurons were also incubated with **HyNDA-1** in the presence of either TAT-D3R or TAT-β2 peptides or their corresponding scrambled peptides (1 μM) (Fig. 7 E-H). As shown for mouse mDA neurons, interfering peptides, but not the scrambled ones, counteracted **HyNDA-1**-induced morphological changes also in hiPSC-derived mDA neurons, and these data suggest that the D3R-nAChR heteromer is most likely expressed also in human DA neurons. Likewise, in this model **HyNDA-1** may elicit morphological remodeling by specifically

targeting the D3R-nAChR complex through activation of both D3R and nAChR protomers forming the heterodimer.

Figure 7 *about here*

3.3.5. ***HyNDA-1*** *increases the affinity of interaction between β2-nAChR and D3R*

Ligands targeting GPCR heterodimers may influence heterodimerization either reducing or increasing the probability for the two protomers to interact [44]. We evaluated the affinity of interaction of D3R for β2 nAChR in response to **HyNDA-1** by means of the $BRET^2$ assay, a bioluminescence technique widely used to study protein-protein interaction in living cells that takes advantage of the transfer of energy from a donor to an acceptor molecule [45]. With $BRET^2$, we demonstrated the existence of a direct interaction between D3R and the β2 subunit of nAChR in living HEK-293 transfected cells [21]. HEK-293 cells were transfected with a fixed amount of β2 subunit fused to the donor RLuc (Beta2Rluc) and an increasing amount of D3R fused to the GFP2 acceptor, previously shown to generate a hyperbolic increase of the $BRET^2$ signals, indicative of a direct and specific protein-protein interaction [21]. Cells were incubated with **HyNDA-1** (1 μM) for 5 min and analyzed for $BRET^2$ signal, compared to untreated cells. As shown in Fig. 8, **HyNDA-1** (Fig. 8B) caused a significant decrease of the $BRET_{50}$ value, corresponding to the $BRET^2$ ratio at which the $BRET^2$ value is 50% of the maximal level (**HyNDA-1**: K_d = 0.74 ± 0.22 *vs.* K_d = 1.67 ± 0.39 with the vehicle), indicating that the D3R interactions with the β2 subunit of nAChR are significantly enhanced in the presence of this ligand.

Figure 8 *about here*

4. Discussion

The propensity of GPCRs to form dimeric and higher order oligomers in natural tissues has drastically changed the vision of this class of receptors, with relevant implications both on basic and translational research [2-4]. On these premises, the development of pharmacological tools selectively targeting heterodimers would be beneficial to delineating localization, function and pharmacology of each dimeric complexes. Moreover, targeting GPCR heterodimers may impact on drug discovery strategies, since dimeric complexes are likely formed in a tissue-specific way, thus paving the way to the design of more selective and efficacious drug candidates with reduced side effects [5,6].

Among heterodimers, the D3R-nAChR complex, involving the direct interaction between a GPCR, the D3R subtype, and the β2 subunit of a nicotinic ion channel (nAChR), was recently characterized through BRET assays in D3R-luc and β2-nAChR-GFP expressing HEK-293 cells and proximity ligation assay (PLA) in mouse DA neurons [21]. Moreover, evidence that both individual D3R and nAChR and their interaction to form the heterodimer are an essential prerequisite for supporting structural plasticity in mouse DA neurons in response to nicotine has been provided [21]. In particular, while stimulation of D3R causes neurotrophic effects "per se" [46,20,40], α4β2 nAChR gains the ability to induce structural plasticity on DA neurons only when is coupled to D3R. Therefore, it is likely that, when activated, the D3R-nAChR complex is the molecular entity that supports DA neurons remodeling, while the D3R should trigger intracellular signals specifically responsible for this effect [20,21, 40]. In neuronal cultures, nicotine-induced neuroplasticity is a long term event [20,21,40]. Numerous lines of evidence have shown that nAChRs subtypes, including the β2-containing nAChR, are functionally upregulated following prolonged exposure to nicotine [47]. Moreover, the membrane expression of D3R is only marginally modified by agonist stimulation [48], thus suggesting that the D3R-nAChR heteromer could be expressed at the neuronal plasma membrane for long terms under nicotine stimulation. However, both signaling and trafficking properties of the D3R-nAChR heteromer need to be elucidated yet. Nevertheless, the remodeling properties of the D3R-nAChR heteromer is a downstream biological event that could represent a "dimer fingerprint" [49] for the D3R-nACR heteromer, i.e., a specific functional property exhibited by the nAChR monomer inside the complex but not associated to the individual receptor subtype.

As previously underlined, in this work we aimed at identifying new molecular probes able to target and stimulate the D3R-nAChR complex. The designed derivatives were synthesized and initially tested in radioligand binding assays at both D3R and native nAChRs. We found that **1a** (**HyNDA-1**), **1b** and **1c** retained a nanomolar affinity for D3R, typical of high affinity reference agonists; moreover, they displayed high affinity for α4β2 nAChRs and low affinity for α3β4 or α7 nAChR subtypes. This behavior is suggestive of the compounds' ability to bind D3R or nAChR either when the two receptors are individually expressed or when they interact to form the D3R-nAChR complex. Such ligands, in fact, incorporating potent and subtype-specific pharmacophoric fragments, could be rationally able to simultaneously bind both protomers of the D3R-nAChR heteromer. We further investigated **HyNDA-1** by taking advantage of the unique ability of the complex under

study to give rise to neurotrophic effects on DA neurons. Moreover, theoretical calculations of ADME parameters and pharmacokinetic properties performed on **HyNDA-1** demonstrated that this hybrid compound is able to cross the blood brain barrier (data not published) [50].

In a preliminary set of experiments, carried out in mouse TH-positive mDA neurons endogenously expressing the D3R-nAChR heteromers [21], we showed that chronic treatment with **HyNDA-1** as well as the individually given nicotinic and D3R agonists significantly induced neurotrophic morphological changes in mDA neurons, measured as maximal length of the primary dendrites, the dendrite number and the soma area. By contrast, a cell toxicity was observed by treating neurons with different concentrations of both **1b** and **1c**. Moreover, while low doses of **HyNDA-1** did not cause any structural modification on mDA neurons, a tenfold higher concentration induced significant morphological changes. These effects were observed starting from 24 h of treatment and reached a peak at 72h; however, at 5 μM even **HyNDA-1** was found to be toxic. Therefore, although the range of concentration was very narrow, we found that **HyNDA-1** is the only hybrid ligand retaining the ability of nicotine to induce structural plasticity on mDA neurons, thus indicating that this compound specifically targets the D3R-nAChR complex. Being aware of the limitations intrinsic to these results, we chose however to further study the properties of **HyNDA-1**, endowed with neurotrophic activity, in the concentration range at which this ligand is devoid of toxic effects.

The role of both protomers of the D3R-nAChR dimer in mediating **HyNDA-1**-induced structural plasticity was next evaluated in mouse mDA neurons by applying D3R and α4β2 nAChR antagonists. Incubation with the D2R/D3R antagonist sulpiride, that hinders **HyNDA-1** binding to the D3R protomer, significantly affected the ability of **HyNDA-1** to exert neurotrophic effects. Similarly, mecamylamine or dihydro-β-erythroidine, hampering **HyNDA-1** interaction with the nAChR recognition site, considerably prevented **HyNDA-1**-induced neurotrophic effects. Therefore, blockage of one or the other binding site of the D3R-nAChR complex negatively affected the ability of **HyNDA-1** to trigger morphological changes. This is in line with the so called "cross antagonism" characterizing some GPCR heterodimers, in which the antagonist of one protomer prevents the activation response promoted by a ligand selectively binding to the other protomer [51]. Overall, these data further support the behavior of **HyNDA-1** as a ligand that specifically targets the heteromer under study. Since disrupting the D3R-nAChR complex in mouse mDA neurons by means of specific D3R-nAChR interfering

peptides [21] precluded any **HyNDA-1**-promoted neurotrophic events, it is indisputable that **HyNDA-1** recognizes and activates the heterodimeric complex.

The molecular features of ligands designed to bridge the space between receptor dimers, thus allowing a simultaneous interaction with both individual protomers, have been studied in-depth for "dimeric" ligands acting on mu and delta opioid (MOP and DOP, respectively) receptor heteromers [52,53]. Molecular modeling and binding studies indicated that the optimal distance between the active sites of individual receptors is around 25 Å for most opioid receptor dimers [52]. In addition to the length, further physicochemical properties of the spacer (such as molecular size and flexibility, hydrophobicity and sensitivity to the action of enzymes) affect the recognition process and, as a consequence, the efficacy of bivalent ligands. At least for GPCR opioid heterodimers, a few studies have also shown that ideal linker lengths for the same bivalent ligands may vary depending on the studied cell model, thus pointing to a critical role of the cell background on receptor dimerization [52,53]. However, we are unaware of detailed studies on the length and nature of spacers linking heteromeric receptor complexes involving GPCRs and ionotropic channels. Interestingly, by using the BRET assay in transfected cells, appropriate bivalent ligands, according to their spacer length, induced "de novo" MOP and cholecystokinin 2 (CCK2) receptor heterodimerization through a bridging mechanism [54]. Our data, showing that in BRET experiments **HyNDA-1** significantly increases the interaction between the D3R and the β2 subunit of nAChR, should reflect the ability of **HyNDA-1** of bridging the two interacting protomers, although the spacer connecting the ligand pharmacophoric portions is predictably too short for such a molecular mechanism. In any case, further studies need to be performed to delineate the mode of action, as a dual acting or as a bivalent ligand, of this archetypal hybrid compound, In this respect, the availability of the crystal structures for both D3R [55] and α4β2 nAChR [56,57] combined with existing molecular modeling approaches, may help gain detailed information on the architecture of the D3R-nAChR dimer, thus allowing a design strategy for truly acting bivalent ligands on a more rational basis.

In summary, our data on **HyNDA-1** represent the initial framework to develop new molecularly hybrid tools enabling the specific detection and/or activation of the D3R-nAChR complex in natural tissues both in vitro and in vivo. Such compounds, recognizing the two orthosteric binding sites of one heteromer, should have the advantage of a higher degree of tissue selectivity over ligands containing the same pharmachophoric moieties within two separate ligands: only tissues expressing both receptor protomers should be, in fact,

targeted by such molecules, implying a potential reduction in the incidence of side effects. Intriguingly, the ability of **HyNDA-1** to exert neurotrophic effects was also evidenced in human cultures containing mDA neurons and derived from iPSC of healthy subjects [40]. We recently found that in human neurons nicotine shows remodeling activity, an effect abolished by D2R/D3R antagonists and suggestive of the existence of a functional crosstalk between nAChRs and the D3Rs [40]. As found in mouse mDA neurons, we demonstrate that **HyNDA-1** significantly increased dendrite length and number, and the soma area of human mDA neurons, an effect prevented by both D2R/D3R and nAChR antagonists and by perturbing the specific association of D3R with nAChR by means of interfering peptides. Therefore, **HyNDA-1** may open the way to designing novel and more potent drug candidates that, acting selectively on the D3R/nAChR heteromer, exhibit neurotrophic properties useful to support DA neurons plasticity and survival against toxic damages in various pathologies such as Parkinson's disease.

Acknowledgments

This work was supported by grants from MIUR (Ministero dell'Istruzione, dell'Università e della Ricerca) - Italy (prot. 2009R7WCZS_002) and from the Universities of Brescia and Milan. We thank Veronica Mutti for her technical contribution.

References

[1] C. Missale, S.R. Nash, S.W. Robinson, M. Jaber, M.G. Caron, Dopamine receptors: from structure to function, Physiol. Rev. 78 (1998) 189-225.

[2] S.R. George, B.F. O'Dowd, S.P. Lee, G-protein-coupled receptor oligomerization and its potential for drug discovery, Nat. Rev. Drug Discov. 1 (2002) 808-820. doi: 10.1038/nrd913

[3] G. Milligan, G protein-coupled receptor hetero-dimerization: contribution to pharmacology and function, Br. J. Pharmacol. 158 (2009) 5-14. doi: 10.1111/j.1476-5381.2009.00169.x

[4] I. Gomes, M.A. Ayoub, W. Fujita, W.C. Jaeger, K.D.C. Pfleger, L.A. Devi, G protein-coupled receptor heteromers, Annu. Rev. Pharmacol. Toxicol. 56 (2016) 403-425. doi: 10.1146/annurev-pharmtox-011613-135952

[5] D. Wacker, R.C. Stevens, B.L. Roth, How ligands illuminate GPCR molecular pharmacology, Cell 170 (2017) 414-421. doi: http://dx.doi.org/10.1016/j.cell.2017.07.009

[6] B. Farran, An update on the physiological and therapeutic relevance of GPCR oligomers, Pharmacol. Res. 117 (2017) 303-327. doi: http://dx.doi.org/10.1016/j.phrs.2017.01.008

[7] C. Missale, C. Fiorentini, The neurobiology of dopamine receptors: evolution from the dual concept to heterodimer complexes, J. Recept. Sig. Transd. 30 (2010) 347-354. doi: http://dx.doi.org/10.3109/10799893.2010.506192

[8] S.R. George, A. Kern, R.G. Smith, R. Franco, Dopamine receptor heteromeric complexes and their emerging functions, Prog. Brain Res. 211 (2014) 183-200. doi: 10.1016/B978-0-444-63425-2.00008-8

[9] C. Fiorentini, C. Busi, P. Spano, C. Missale, Role of receptor heterodimers in the development of L-DOPA-induced dyskinesias in the 6-hydroxydopamine rat model of Parkinson's disease, Parkinsonism Relat. Disord. 14 Suppl 2 (2008) S159-164. doi: 10.1016/j.parkreldis.2008.04.022.

[10] C. Fiorentini, P. Savoia, D. Savoldi, C. Missale, Receptor heteromers in Parkinson's disease and L-DOPA-induced dyskinesia, CNS Neurol. Disord. Drug Targets. 12 (2013) 1101-1113. doi: 10.2174/18715273113120011 8

[11] B.E. McKay, A.N. Placzek, J.A. Dani, Regulation of synaptic transmission and plasticity by neuronal nicotinic acetylcholine receptors, Biochem. Pharmacol. 74 (2007) 1120-1133. doi: 10.1016/j.bcp.2007.07.001

[12] J-P. Changeux, The nicotinic acetylcholine receptor: the founding father of the pentameric ligand-gated ion channel superfamily, J. Biol. Chem. 287 (2012) 40207-40215. doi: 10.1074/jbc.R112.407668.

[13] D. Manetti, C. Bellucci, N. Chiaramonte, S. Dei, E. Teodori, M.N. Romanelli, Designing selective modulators for the nicotinic receptor subtypes: challenges and opportunities, Future Med. Chem. 10 (2018) 433-459. doi: https://doi.org/10.4155/fmc-2017-0169

[14] C. Gotti, S. Guiducci, V. Tedesco, S. Corbioli, L. Zanetti, M. Moretti, A. Zanardi, R. Rimondini, M. Mugnaini, F. Clementi, C. Chiamulera, M. Zoli, Nicotinic acetylcholine receptors in the mesolimbic pathway: primary role of ventral tegmental area α6β2* receptors in mediating systemic nicotine effects on dopamine release, locomotion, and reinforcement, J. Neurosci. 30 (2010) 5311-5325. doi: https://doi.org/10.1523/JNEUROSCI.5095-09.2010

[15] H. Fischer, D-M Liu, A. Lee, J.C. Harries, D.J. Adams, Selective modulation of neuronal nicotinic acetylcholine receptor channel subunits by G_o-protein subunits, J. Neurosci. 25 (2005) 3571-3577. doi: https://doi.org/10.1523/JNEUROSCI.4971-04.2005

[16] J.C. Nordman, N. Kabbani, An interaction between α7 nicotinic receptors and a G protein pathway complex regulates neurite growth in neural cells, J. Cell Sci. 125 (2012) 5502-5513. doi: 10.1242/jcs.110379

[17] N. Kabbani, J.C. Nordman, B.A. Corgiat, D.P. Veltri, A. Shehu, V.A. Seymour, D.J. Adams, Are nicotinic acetylcholine receptors coupled to G proteins?, Bioessays 35 (2013) 1025-1034, and references cited therein. doi:10.1002/bies.201300082

[18] J.G. Partridge, S. Apparsundaram, G.A. Gerhardt, J. Ronesi and D.M. Lovinger, Nicotinic acetylcholine receptors interact with dopamine in induction of striatal long-term depression, J. Neurosci. 22 (2002), 2541-2549; doi: 10.1523/JNEUROSCI.22-07-02541.2002

[19] D. Quarta, F. Ciruela, K. Patkar, J. Borycz, M. Solinas, C. Lluis, R. Franco, R. Wise, S.R. Goldberg, B.T. Hope, A.S. Woods, S. Ferré, Heteromeric nicotinic acetylcholine-dopamine autoreceptor complexes modulate striatal dopamine release, Neuropsychopharmacol. 32 (2007) 35-42. doi: http://dx.doi.org/ 10.1038/sj.npp.1301103

[20] G. Collo, F. Bono, L. Cavalleri, L. Plebani, S. Mitola, E. M. Pich, M. J. Millan, M. Zoli, U. Maskos, P. Spano, C. Missale, Nicotine-induced structural plasticity in mesencephalic dopaminergic neurons is mediated by dopamine D3 receptors and Akt-mTORC1 signaling, Mol. Pharmacol. 83 (2013) 1176-1189. doi: 10.1124/mol.113.084863

[21] L. Bontempi, P. Savoia, F. Bono, C. Fiorentini, C. Missale, Dopamine D3 and acetylcholine nicotinic receptor heteromerization in midbrain dopamine neurons: relevance for neuroplasticity, Eur. Neuropsychopharm. 27 (2017) 313-324. doi: http://dx.doi.org/10.1016/j.euroneuro.2017.01.015

[22] C. Fiorentini, P. Savoia, F. Bono, P. Tallarico, C. Missale, The D3 dopamine receptor: from structural interactions to function, Eur. Neuropsychopharm. 25 (2015) 1462-1469. doi: https://doi.org/10.1016/j.euroneuro.2014.11.021

[23] A. Bock, B. Chirinda, F. Krebs, R. Messerer, J. Bätz, M. Muth, C. Dallanoce, D. Klingenthal, C. Tränkle, C. Hoffmann, M. De Amici, U. Holzgrabe, E. Kostenis, K. Mohr, Dynamic ligand binding dictates partial agonism at a G protein-coupled receptor, Nat. Chem. Biol. 10 (2014) 18-20. doi: 10.1038/nchembio.138

[24] C. Matera, L. Flammini, M. Quadri, V. Vivo, V. Ballabeni, U. Holzgrabe, K. Mohr, M. De Amici, E. Barocelli, S. Bertoni, C. Dallanoce, Bis(ammonio)alkane-type agonists of muscarinic acetylcholine receptors: Synthesis, in vitro functional characterization, and in vivo evaluation of their analgesic activity, Eur. J. Med. Chem. 75 (2014) 222-232. doi: 10.1016/j.ejmech.2014.01.032

[25] A. Bock, M. Bermudez, F. Krebs, C. Matera, B. Chirinda, D. Sydow, C. Dallanoce, U. Holzgrabe, M. De Amici, M.J. Lohse, G. Wolber, K. Mohr, Ligand binding ensembles determine graded agonist efficacies at a G protein-coupled receptor, J. Biol. Chem. 291 (2016) 16375-16389. doi: https://doi.org/10.1074/JBC.M116.735431

[26] C. Matera, L. Pucci, C. Fiorentini, S. Fucile, C. Missale, G. Grazioso, F. Clementi, M. Zoli, M. De Amici, C. Gotti, C. Dallanoce, Bifunctional compounds targeting both D2 and non-α7 nACh receptors: design, synthesis and pharmacological characterization, Eur. J. Med. Chem. 101 (2015) 367-383. doi: 10.1016/j.ejmech.2015.06.039

[27] R. Morphy, Z. Rankovic, The physicochemical challenges of designing multiple ligands, J. Med. Chem. 49 (2006) 4961-4970. doi: 10.1021/jm0603015

[28] T.W. Corson, N. Aberle, C.M. Crews, Design and applications of bifunctional small molecules: why two heads are better than one, ACS Chem. Biol. 3 (2008) 677-692. doi: 10.1021/cb8001792

[29] J. Shonberg, P.J. Scammells, B. Capuano, Design strategies for bivalent ligands targeting GPCRs, ChemMedChem 6 (2011) 963-974. doi: 10.1002/cmdc.201100101

[30] H. Hübner, T. Schellhorn, M. Gienger, C. Schaab, J. Kaindl, L. Leeb, T. Clark, D. Möller, P. Gmeiner, Structure-guided development of heterodimer-selective GPCR ligands, Nat. Commun. 7 (2016) 12298. doi: 10.1038/ncomms12298

[31] M. Jörg, L. May, F.S. Mak, K.C. Lee, N.D. Miller, P.J. Scammels, B. Capuano, Synthesis and pharmacological evaluation of dual acting ligands targeting the adenosine A2A and dopamine D2 receptors for the potential treatment of Parkinson's disease, J. Med. Chem. 58 (2015) 718-738. doi:10.1021/jm501254

[32] M. Glass, K. Govindpani, D.P. Furkert, D.P. Hurst, P.H. Reggio, J.U. Flanagan, One for the price of two … Are bivalent ligands targeting cannabinoid receptor dimers capable of simultaneously binding to both receptors?, Trends Pharmacol. Sci. 37 (2016) 353-363. doi: 10.1016/j.tips.2016.01.010

[33] M.A. Abreo, N.H. Lin, D.S. Garvey, D.E. Gunn, A.M. Hettinger, J.T. Wasicak, P.A. Pavlik, Y.C. Martin, D.L. Donnelly-Roberts, D.J. Anderson, J.P. Sullivan, M. Williams, S.P. Arneric, M.W..Holladay, Novel 3-pyridyl ethers with subnanomolar affinity for central neuronal nicotinic acetylcholine receptors, J. Med. Chem. 39 (1996) 817-825. doi:10.1021/jm9506884

[34] N.H. Lin, Y. Li, Y. He, M.W. Holladay, T. Kuntzweiler, D.J. Anderson, J.E. Campbell, S.P. Arneric, Synthesis and structure–activity relationships of 5-substituted pyridine analogues of 3-[2-((*S*)-pyrrolidinyl)methoxy]pyridine, A-84543: a potent nicotinic receptor ligand, Bioorg. Med. Chem. Lett. 11 (2001) 631-633. doi: 10.1016/s0960-894x(01)00030-0

[35] Z.L. Wei, Y. Xiao, H. Yuan, M. Baydyuk, P.A. Petukhov, J.L. Musachio, K.J. Kellar, A.P. Kozikowski, Novel pyridyl ring C5 substituted analogues of Epibatidine and 3-(1-Methyl-2(*S*)-pyrrolidinylmethoxy)pyridine (A-84543) as highly selective agents for neuronal nicotinic acetylcholine receptors containing β2 subunits, J. Med. Chem. 48 (2005) 1721-1724. doi:10.1021/jm0492406

[36] M.C. Coldwell, I. Boyfield, T. Brown, J.J. Hagan, D.N. Middlemiss, Comparison of the functional potencies of ropinirole and other dopamine receptor agonists at human $D_{2(long)}$, D_3 and $D_{4.4}$ receptors expressed in Chinese hamster ovary cells, Brit. J. Pharmacol. 127 (1999) 1696-1702. doi:10.1038/sj.bjp.0702673

[37] F. Du, R. Li, Y. Huang, X. Li, W. Le, Dopamine D3 receptor-preferring agonists induce neurotrophic effects on midbrain dopamine neurons, Eur. J. Neurosci. 22 (2005) 2422-2430. doi:10.1111/j.1460-9568.2005.04438.x

[38] M. Jörg, A.A. Kaczor, F.S. Mak, K.C.K. Lee, A. Poso, N.D. Miller, P.J. Scammels, B. Capuano, Investigation of novel ropinirole analogues: synthesis, pharmacological evaluation and computational analysis of dopamine D_2 receptor functionalized congeners and homobivalent ligands, MedChemComm 5 (2014) 891-898. doi:10.1039/c4md00066h

[39] C. Matera, M. Quadri, S. Pelucchi, M. De Amici, C. Dallanoce, A convenient synthesis of 4-(2-hydroxyethyl)indolin-2-one, a useful intermediate for the preparation of both dopamine receptor

agonists and protein kinase inhibitors, Monatsh. Chem. 145 (2014) 1139-1144. doi: 10.1007/s00706-014-1211-z

[40] F. Bono, P. Savoia, A. Guglielmi, M. Gennarelli, G. Piovani, S. Sigala, D. Leo, S. Espinoza, R.R. Gainetdinov, P. Devoto, P. Spano, C. Missale, C. Fiorentini, Role of dopamine D2/D3 receptors in development, plasticity, and neuroprotection in human iPSC-derived midbrain dopaminergic neurons, Mol. Neurobiol. 55 (2018) 1054-1067. doi: 10.1007/s12035-016-0376-3P

[41] J. Munson, D. Rodbard, Ligand: a versatile computerized approach for characterization of ligand-binding systems, Anal. Biochem. 107 (1980) 220e239.

[42] K. Hidaka, S. Tada, M. Matsumoto, J. Ohmori, Y. Tasaki, T. Nomura, S. Usuda, T. Yamaguchi, In vitro pharmacological profile of YM-43611, a novel D2-like receptor antagonist with high affinity and selectivity for dopamine D3 and D4 receptors, Br. J. Pharmacol. 117 (1996) 1625–1632.

[43] M.B. Doura, T.V. Luu, N.H. Lee, D.C. Perry, Persistent gene expression changes in ventral tegmental area of adolescent but not adult rats in response to chronic nicotine, Neurosci. 170 (2010) 503-513. doi: 10.1016/j.neuroscience.2010.06.071

[44] K.A. Jacobson, New paradigms in GPCR drug discovery, Biochem. Pharmacol. 98 (2015) 541-555. doi: 10.1016/j.bcp.2015.08.085

[45] A. Bellucci, C. Fiorentini, M. Zaltieri, C. Missale, P.F. Spano, The "in situ" proximity ligation assay to probe protein-protein interactions in intact tissues, Methods Mol. Biol. 1174 (2014) 397-405. doi: 10.1007/978-1-4939-0944-5_27

[46] G. Collo, S. Zanetti, C. Missale, P. Spano, Dopamine D3 receptor-preferring agonists increase dendrite arborization of mesencephalic dopaminergic neurons via extracellular signal-regulated kinase phosphorylation. Eur. J. Neurosci. 28 (2008) 1231-1240. doi: 10.1111/j.1460-9568.2008.06423.x

[47] B. Buisson, D. Bertrand, Nicotine addiction: the possible role of functional upregulation, Trends Pharmacol. Sci. 23 (2002) 130-136. doi: 10.1016/S0165-6147(00)01979-9

[48] K.M. Kim, K.J. Valenzano, S.R. Robinson, W.D. Yao, L.S. Barak, M.G. Caron, Differential regulation of the dopamine D2 and D3 receptors by G protein-coupled receptor kinases and beta-arrestins. J. Biol. Chem. 276 (2001) 37409-37414. doi: 10.1074/jbc.M106728200

[49] R. Franco, V. Casadó, A. Cortés, J. Mallol, F. Ciruela, S. Ferré, C. Lluis, E.I. Canela, G-protein-coupled receptor heteromers: function and ligand pharmacology, Br. J. Pharmacol. 153 (2008), S90-S98. doi:10.1038/sj.bjp.0707571

[50] A. Daina, O. Michielin, V. Zoete, SwissADME: a free web tool to evaluate pharmacokinetics, drug-likeness and medicinal chemistry friendliness of small molecules, Sci. Rep. 7:42717. doi: 10.1038/srep42717 SwissADME: http://www.swissadme.ch/

[51] X. Guitart, G. Navarro, E. Moreno, H. Yano, N.-S. Cai, M. Sánchez-Soto, S. Kumar-Barodia, Y.T. Naidu, J. Mallol, A. Cortés, C. Lluís, E.I. Canela, V. Casadó, P.J. McCormick, S. Ferré, Functional selectivity of allosteric interactions within G protein-coupled receptor oligomers: the dopamine D_1-D_3 receptor heterotetramer, Mol. Pharmacol. 86 (2014) 417-429. doi: 10.1124/mol.114.093096

[52] N. Dietis, R. Guerrini, G. Calo, S. Salvadori, D. J. Rowbotham, D. G. Lambert, Simultaneous targeting of multiple opioid receptors: a strategy to improve side-effect profile, Brit. J. Anaesth. 103 (2009) 38-49, and references cited therein. doi:10.1093/bja/aep129

[53] W. Fujita, I. Gomes, L.S. Dove, D. Prohaska, G. McIntyre, L.A. Devi, Molecular characterization of eluxadoline as a potential ligand targeting mu-delta opioid receptor heteromers, Biochem. Pharmacol. 92 (2014) 448-456. doi: 10.1016/j.bcp.2014.09.015

[54] Y. Zheng, E. Akgün, K.G. Harikumar, J. Hopson, M.D. Powers, M.M. Lunzer, L.J. Miller, P.S. Portoghese, Induced association of mu opioid (MOP) and type 2 cholecystokinin (CCK2) receptors by novel bivalent ligands, J. Med. Chem. 52 (2009) 247-258. doi:10.1021/jm800174p

[55] E.Y. Chien, W. Liu, Q. Zhao, V. Katritch, G.W. Han, M.A. Hanson, L. Shi, A.H. Newman, J.A. Javitch, V. Cherezov, R.C. Stevens, Structure of the human dopamine D3 receptor in complex with a D2/D3 selective antagonist, Science 330 (2010) 1091-1095. doi: 10.1126/science.1197410

[56] C.L. Morales-Perez, C.M. Noviello, R.E Hibbs, X-ray structure of the human α4β2 nicotinic receptor, Nature 538 (2016) 411-415. doi: 10.1038/nature19785

[57] R.M. Walsh Jr., S.H. Roh, A. Gharpure, C.L. Morales-Perez, J. Teng, R.E. Hibbs, Structural principles of distinct assemblies of the human α4β2 nicotinic receptor, Nature 557 (2018) 261-265. doi: 10.1038/s41586-018-0081-7

[58] T. Kvernmo, S. Härtter, E. Burger, A review of the receptor-binding and pharmacokinetic properties of dopamine agonists. Clin. Ther. 28 (2006) 1065-1078. doi: 10.1016/j.clinthera.2006.08.004

Table 1. Affinity data of target compounds **HyNDA-1**, **1b** and **1c** at D3R expressed in HEK cells and at native α4β2, α3β4, and α7 nAChRs present in rat cortical membranes. The reference nicotinic ligand A-84543 was synthesized and tested, whereas data on ropinirole are taken from the literature [58]. The numbers in brackets refer to the % CV. N.t.: not tested.

Entry	D3R [^{3}H]Raclopride K_i (nM)	α4β2 [^{3}H]Epi K_i (nM)	α3β4 [^{3}H]Epi K_i (nM)	α7 [^{125}I]α-Bgtx K_i (nM)
HyNDA-1	3.8 (11.5%)	4.50 (26%)	125 (42%)	11,600
1b	18 (7.8%)	1.22 (24%)	681 (45%)	26,800
1c	2.6 (18.5%)	1.72 (22%)	1,100 (49%)	4,300
A-84543	N.t.	1.20 (17%)	1,900	58 (26%)
Ropinirole	2.9	N.t.	N.t.	N.t.

Table 1
(C. Matera et al.)

(β2*)nAChR agonists

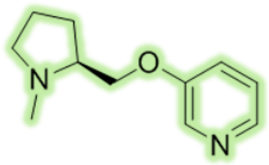

A-84543

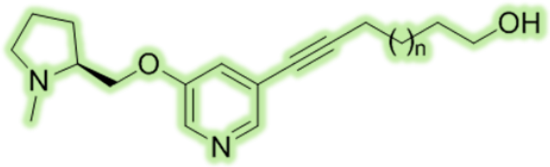

n = 1, 5 (ref. 28)

D3R agonist

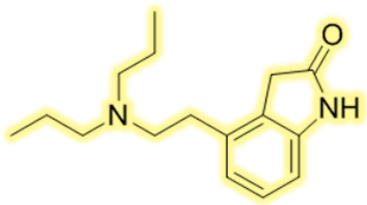

Ropinirole

hybrid agonists

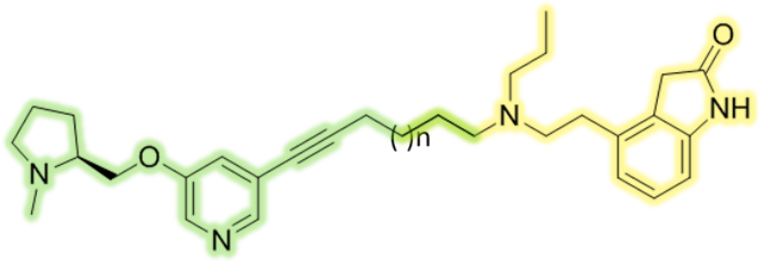

1a (**HyNDA-1**, n=1), **1b** (n=3), **1c** (n=5)

Figure 1
(C. Matera et al.)

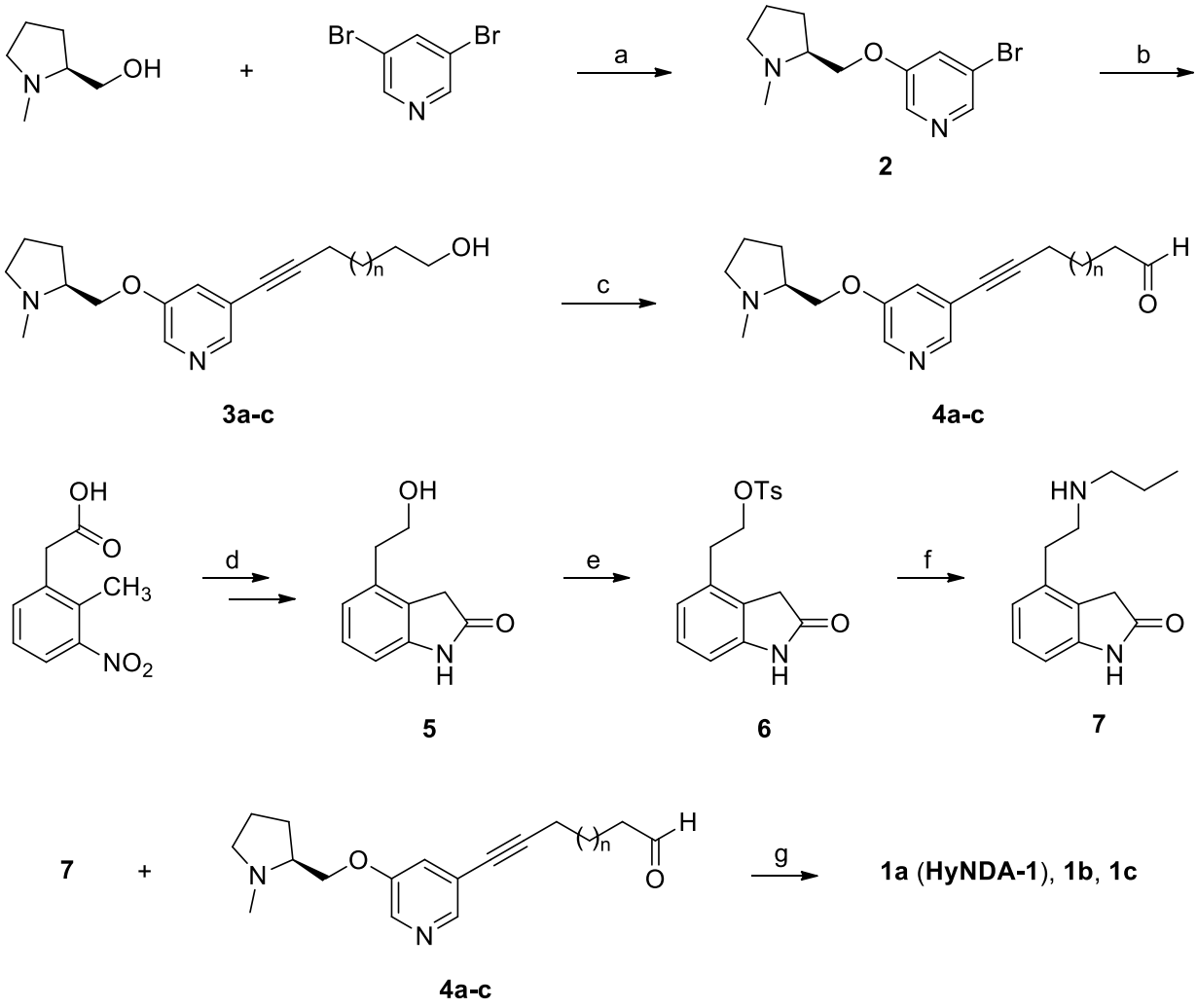

Figure 2
(C. Matera et al.)

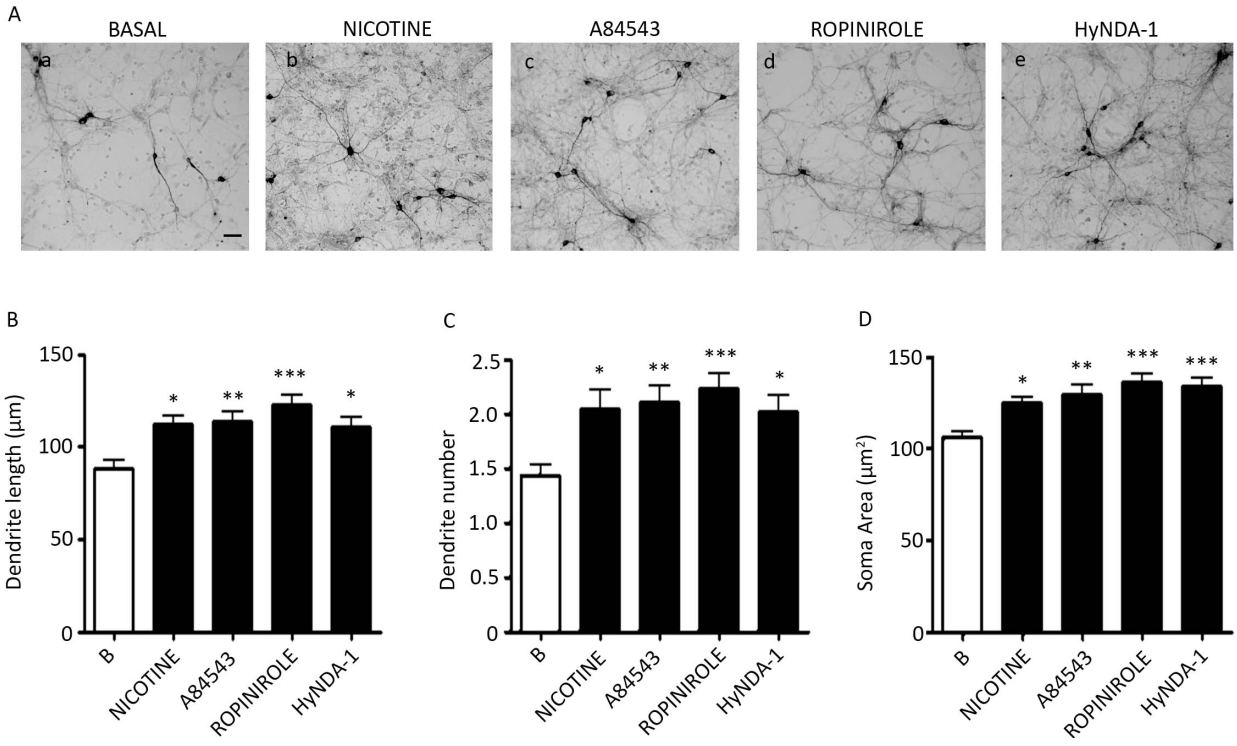

Figure 3
(C. Matera et al.)

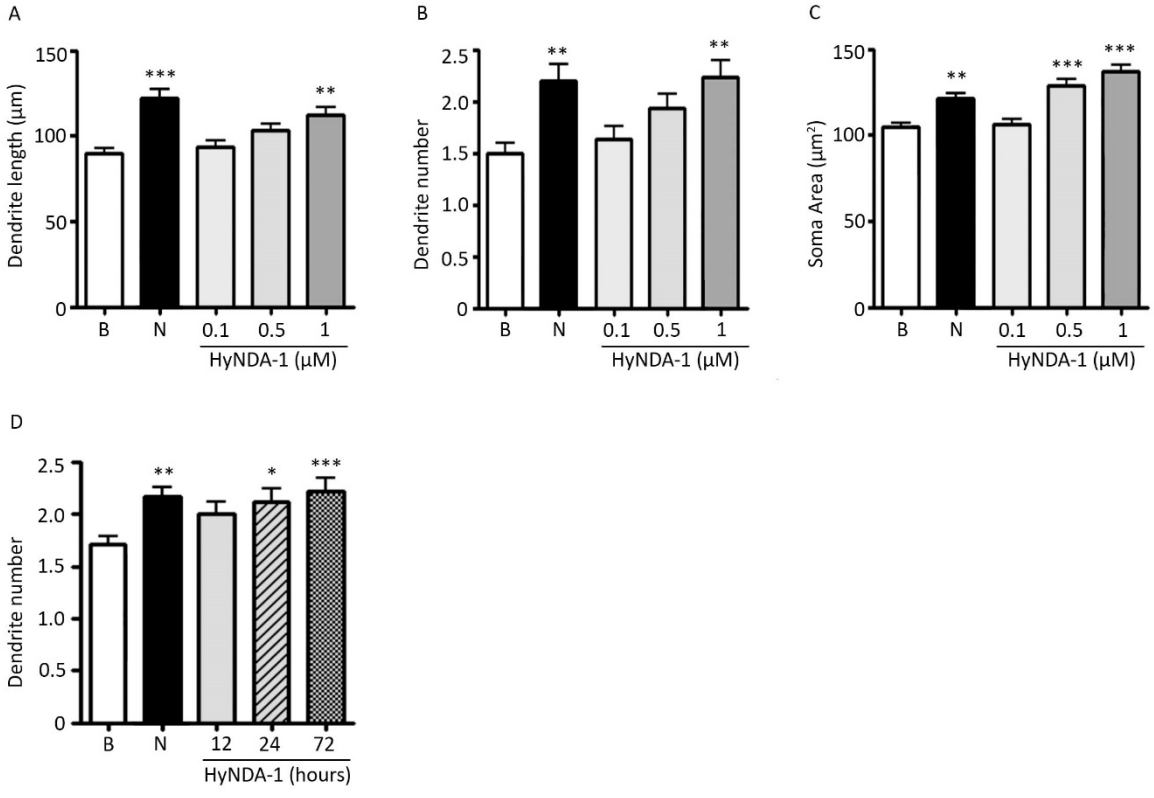

Figure 4
(C. Matera et al.)

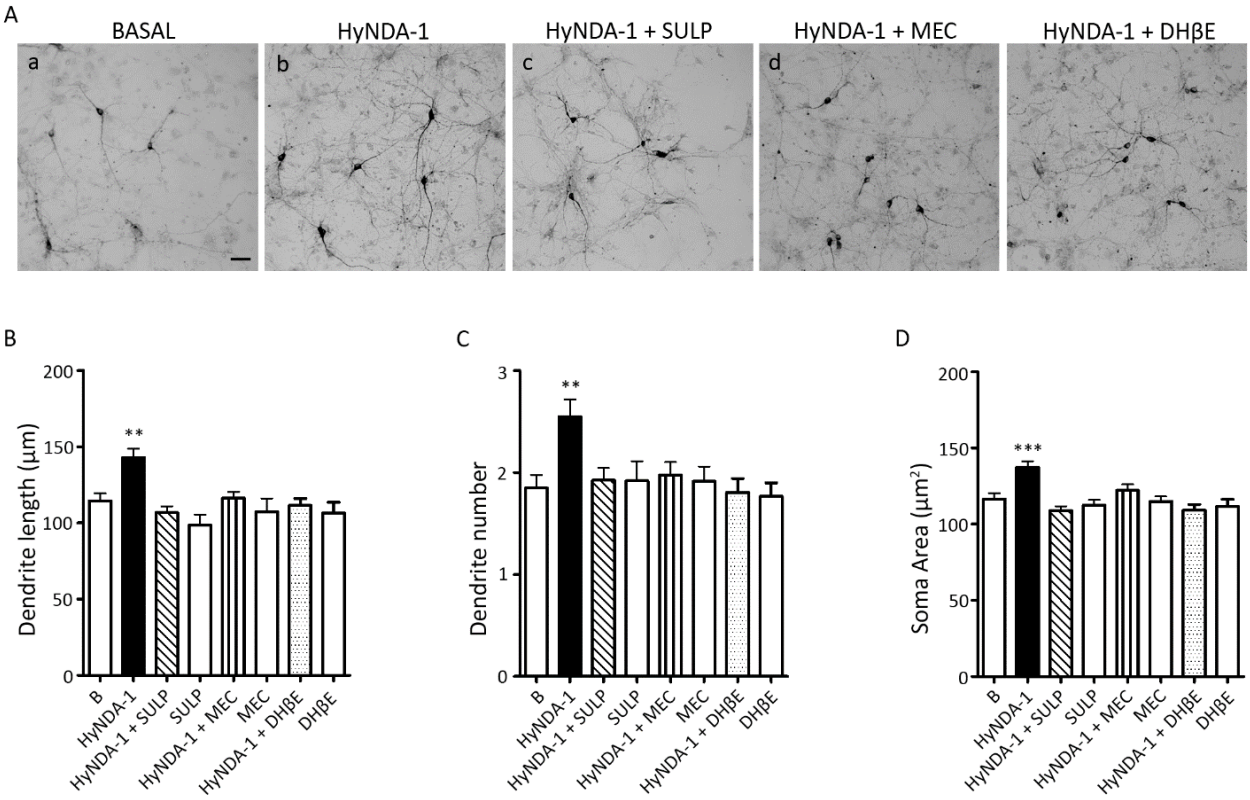

Figure 5
(C. Matera et al.)

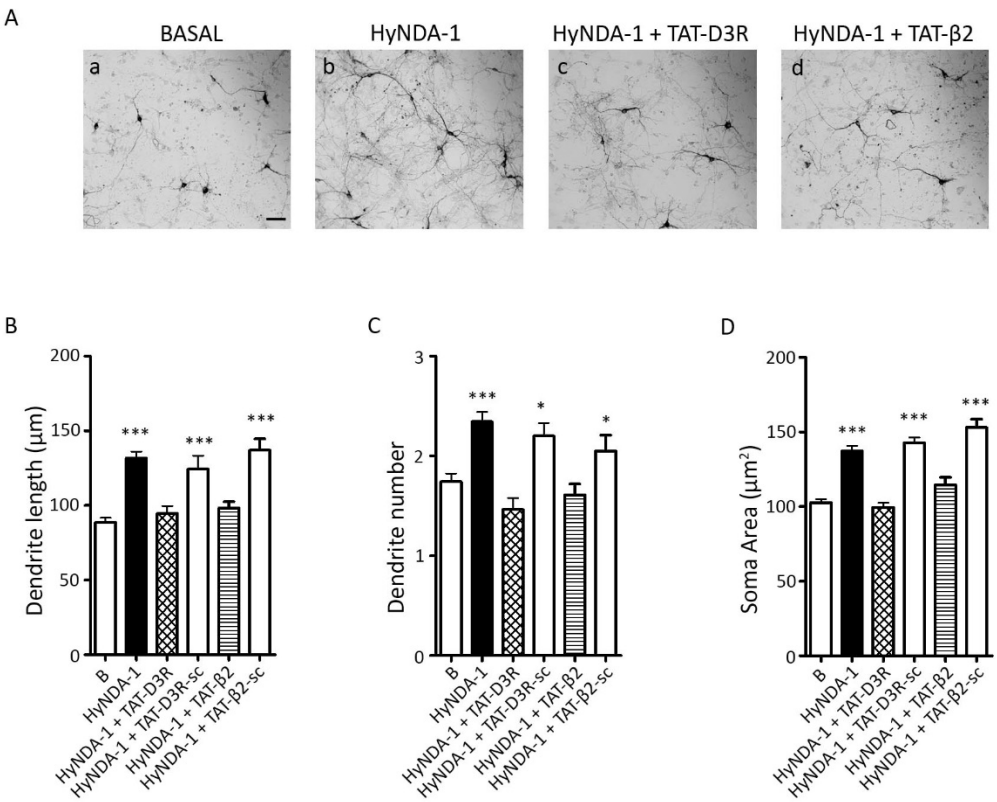

Figure 6
(C. Matera et al.)

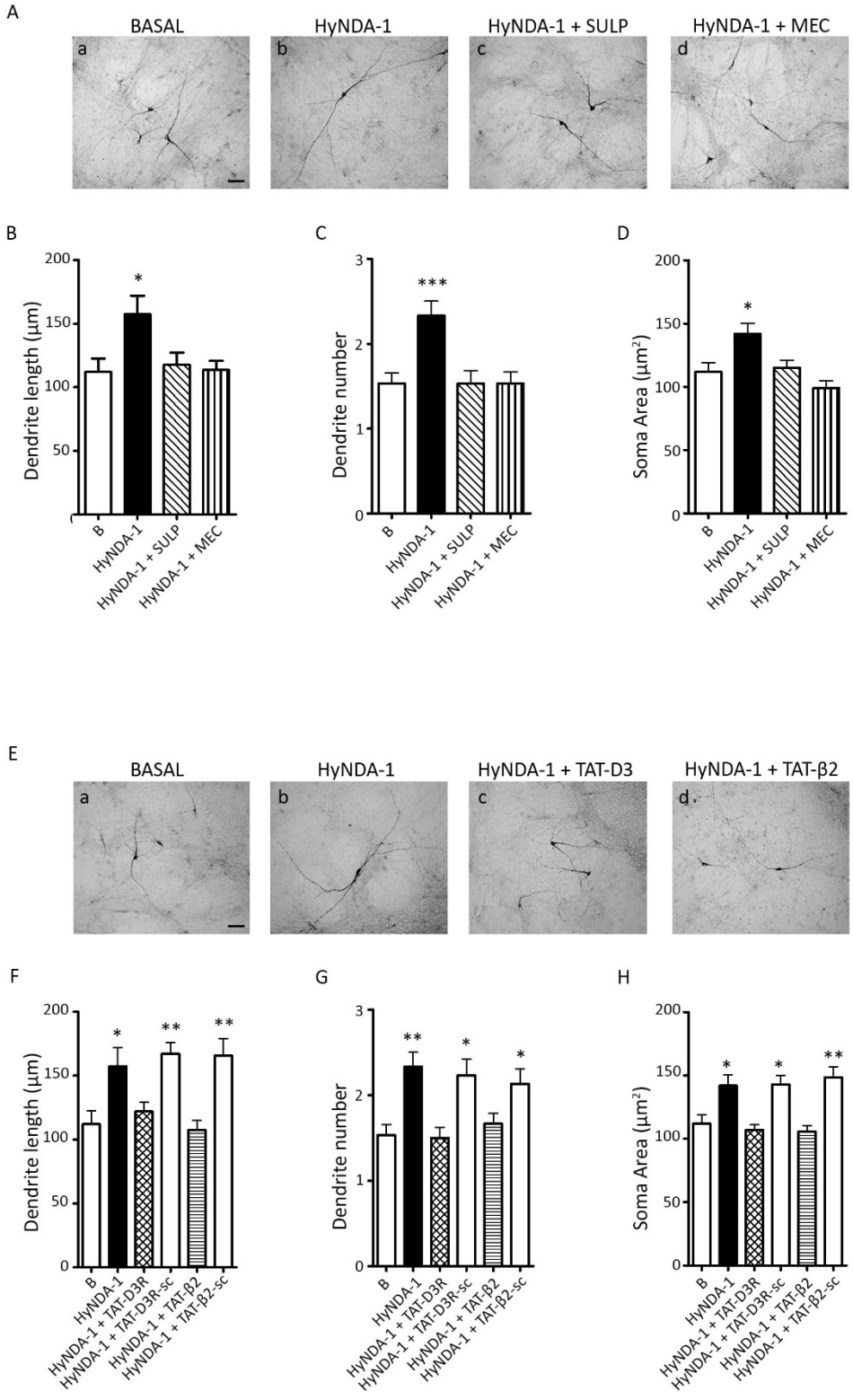

Figure 7
(C. Matera et al.)

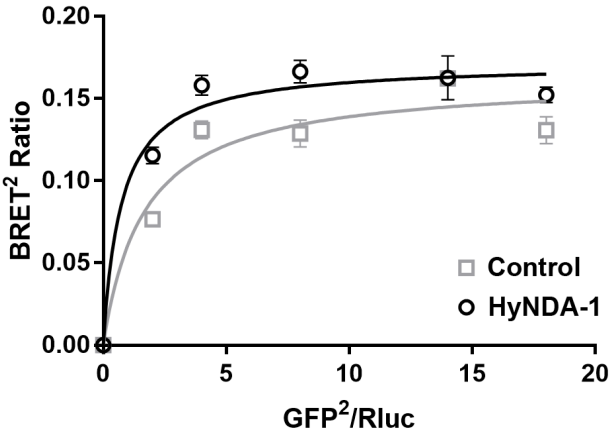

Figure 8
(C. Matera et al.)

Captions to Figures and Schemes

Fig. 1. Structures of the designed, putative D3R-(β2*)nAChR agonists **1a-c** and their parent compounds.

Fig. 2. *Reagents and conditions:* (a) NaH, anhydrous DMF, r.t., 48 h; (b) alkynyl alcohol, 10% Pd-C, CuI, PPh_3, K_2CO_3, DME, H_2O, reflux, 72 h (n = 1 for **3a**; n = 3 for **3b**, n = 5 for **3c**); (c) Dess-Martin periodinane, anhydrous CH_2Cl_2, r.t., 4 h (n = 1 for **4a**; n = 3 for **4b**, n = 5 for **4c**); (d) see reference [39]; (e) *p*-toluenesulfonyl chloride, pyridine, anhydrous CH_2Cl_2, 0 °C to r.t., 4 h; (f) *n*-propylamine, reflux, 1 h; (g) $NaBH_3CN$, anhydrous MeOH, r.t., 1 h.

Fig. 3. Morphological effects of nicotine, A-84543, ropinirole and **HyNDA-1** on mouse mDA neurons. Mouse neurons were incubated with nicotine (10 μM), A-84543 **(**10 μM), ropinirole (10 μM) and **HyNDA-1** (1 μM) for 72 h and analyzed for morphological changes by using immunocytochemistry. DA neurons were visualized using a primary antibody raised against the tyrosine hydroxylase (TH) enzyme. (A) Representative micrographs of TH-immunoreactive (TH-IR) neurons following 72 h exposure to basal (a), nicotine (b), A-84543 (c), ropinirole (d) or **HyNDA-1** (e). Scale bar: 60 μm. (B-D) Quantitative analyses of nicotine, A-84543, ropinirole and **HyNDA-1** effect on maximal dendrite length (B), number of primary dendrites (C), and soma area (D). In all panels, values are represented as mean ± standard error of the mean (SEM) of three independent experiments (** $p < 0.01$; *$p < 0.05$ vs. basal, post hoc Bonferroni's test). B: basal.

Fig. 4. Effect of **HyNDA-1** on mouse mDA neurons. Mouse neuronal cultures were incubated with nicotine (10 μM) and with increasing concentration of **HyNDA-1** (0.1, 0.5, 1.0 μM) for 72 h, and were analyzed for morphological changes (A-C). Quantitative analyses of nicotine (N) and **HyNDA-1** on maximal dendrite length (A), number of primary dendrites (B), and soma area (C) in TH-IR neurons, measured 72 h after treatment. (D) Mouse neuronal cultures were incubated with nicotine (10 μM; 72 h) and with **HyNDA-1** (1 μM) for 12, 24 and 72 h, and TH-IR neurons analyzed for number of primary dendrites. In all panels, values are represented as mean ± standard error of the mean (SEM) of three independent experiments (*** $p < 0.001$; ** $p < 0.01$; *$p < 0.05$ vs. basal, post hoc Bonferroni's test). B: basal; N: nicotine.

Fig. 5. Exposure to D2R/D3R or nAChR antagonists prevents **HyNDA-1**-induced morphological effects on mouse mDA neurons. Mouse neuronal cultures were incubated with **HyNDA-1** (1 μM, 72 h) in the absence or in the presence of sulpiride (10 μM), mecamylamine (50 μM) or dihydro-β-erythroidine (10 μM) and analyzed for morphological changes. Neurons were treated also with sulpiride, mecamylamine or dihydro-β-erythroidine alone, as control (panels B-D) (A) Representative micrographs of TH-IR neurons following 72 h exposure to basal (a), **HyNDA-1** (b), or **HyNDA-1** in combination with sulpiride (c), mecamylamine (d) or dihydro-β-erythroidine (e). Scale bar: 60 μm. (B-D) Quantitative analyses of **HyNDA-1** treatment in combination with sulpiride, mecamylamine or dihydro-β-erythroidine on TH-IR neurons maximal dendrite

length (B), number of primary dendrites (C) and soma area (D). In all panels, values are represented as mean ± standard error of the mean (SEM) of at least three independent experiments (** $p < 0.01$; ***$p < 0.001$ vs. basal, post hoc Bonferroni's test). B: basal; SULP: sulpiride; MEC: mecamylamine; DhβE: dihydro-β-erythroidine.

Fig. 6. The TAT-D3R and TAT-β2 peptide abolishes the morphological effects of **HyNDA-1** on mDA neurons. Mouse neuronal cultures were treated with **HyNDA-1** (1 μM) for 72 h in the presence or the absence of TAT-D3R and TAT-β2 peptides (both at 1 μM), or in the presence of the scrambled TAT-D3R Sc and TAT-β2 Sc peptides (both at 1 μM). Neurons were analyzed for morphological changes. (A) Representative photomicrographs of TH-IR neurons after a 72 h exposure to either basal (a), 1 μM **HyNDA-1** (b), **HyNDA-1** plus TAT-D3R (1 μM) (c) or **HyNDA-1** plus TAT-β2 (1 μM) (d). (B-D) Quantitative analysis of TH-IR neurons maximal dendrite length (B), dendrite number (C) and soma area (D). In all panels, values are represented as mean ± standard error of the mean of four independent experiments (SEM) (* $p < 0.05$; ***$p < 0.001$ vs. basal, post hoc Bonferroni's test). B: basal.

Fig. 7. Effects of **HyNDA-1** on structural plasticity of human iPSC-derived mDA neurons. Human iPSC-derived neuronal cultures were treated with **HyNDA-1** for 72 h in the absence or in the presence of sulpiride (10 μM) or mecamylamine (50 μM), both added 30 min prior to **HyNDA-1** stimulation. TH-positive mDA neurons were analyzed for morphological effects. (A) Representative micrographs of human TH-IR neurons following 72 h exposure to basal (a), **HyNDA-1** (b) or **HyNDA-1** in combination with sulpiride (c) or mecamylamine (d). Scale bar: 60 μm. (B-D) Quantitative analyses of **HyNDA-1** effects in combination with sulpiride or mecamylamine on maximal dendrite length (B), number of primary dendrites (C) and soma area (D). Human iPSC-derived neuronal cultures were incubated with **HyNDA-1** in the presence of TAT-D3R and TAT-β2 peptides (both at 1 μM) and their corresponding TAT-D3R Sc and TAT-β2 Sc scrambled peptides (both at 1 μM). (E) Representative photomicrographs of human TH-IR neurons after a 72 h exposure to either basal (a), **HyNDA-1** (b), **HyNDA-1** plus TAT-D3R (c) or **HyNDA-1** plus TAT-β2 (d). (F-H) Quantitative analysis of maximal dendrite length (F), dendrite number (G) and soma area (H). In all panels, values are represented as mean ± standard error of the mean of three independent experiments (SEM) (*$p < 0.05$; ***$p < 0.001$ vs. basal, post hoc Bonferroni's test). B: basal; SULP: sulpiride; MEC: mecamylamine.

Fig. 8. HyNDA-1 increases the affinity of interaction between D3R and β2 nAChR in HEK-293 transfected cells. HEK-293 cells co-expressing increased amounts of D3R-GFP2 (0.2-1.8 μg) and a fixed amount of Beta2Rluc (0.1 μg) were incubated for 5 min with **HyNDA-1** (1 μM) and analyzed for $BRET^2$ signal, compared to untreated cells and processed for $BRET^2$. $BRET^2_{50}$ values were compared by Extra sum-of-square F test. Data are expressed as means ± SE of twelve independent experiments. $BRET^2$ saturation curves were plotted with GraphPad Prism4 using a linear regression curve assuming one-site binding. *$p < 0.05$ *vs.* untreated cells (control).